AUT Jouranl of Modeling and Simulation

AUT J. Model. Simul., 52(1) (2020) 97-116
DOI: 10.22060/miscj.2020.17306.5178

A Multi-Scale Transform Method Based on Morphological Operators for Pansharpening

Maryam Imani

Faculty of Electrical and Computer Engineering, Tarbiat Modares University, Tehran, Iran

ABSTRACT: The aim of pansharpening is to fuse the low resolution multispectral (MS) image with the high resolution panchromatic (PAN) image to provide a synthesized MS image with high resolution. One of the main approaches for pansharpening is the multi-resolution analysis (MRA). It is generally successful in transform of spectral information. But, it often results in spatial distortion in the fused product. To deal with this problem, a morphological profile based multi-scale transform (MP-MST) is proposed in this paper which utilizes the good characteristics of morphological filters for reduction of spatial redundancies in the pansharpened image. More efficient approximate image and detail image are achieved from the MS and PAN images by applying the closing and opening by reconstruction operators, respectively. Different spatial structures with different sizes are extracted through considering a range of structuring elements sizes. The performance of the proposed MP-MST methods is compared to MST ones by doing experiments on three different remote sensors GeoEye, QuickBird and IKONOS. The experiments show the superior performance of MP-MST method compared to MST in terms of various qualitative assessments. The visual comparison is also investigated. The proposed MP-MST methods solve the problem of noise and redundant spatial information in the pansharpened images significantly.

Review History:
Received: Nov. 01, 2019
Revised: Feb. 21, 2020
Accepted:Feb. 22, 2020
Available Online:Jun. 15, 2020

Keywords:
multi-scale transform
morphology
pansharpening
image fusion

1- INTRODUCTION

Satellite remote sensors can acquire images about the same area of the Earth surface in different wavelengths at different spatial resolutions. The multispectral (MS) sensors acquire images in several spectral bands with a coarse spatial resolution while the panchromatic (PAN) sensors acquire a single band image from the same scene with a fine resolution. While the high spatial resolution of PAN helps to recognize the fine features, the high spectral resolution of MS is required to discriminate among objects with different materials. In respond to requirement to an image with both high spectral resolution and high spatial resolution, fusion of MS and PAN images has been introduced which is known as pansharpening [1].

In the literature, two main groups of pansharpening methods can be seen: the component substitution (CS) methods [2]-[3] and the multi-resolution analysis (MRA) [4]-[5] or multi-scale transform (MST) approaches. The CS methods generally apply a color transform to the MS image to decorrelate spectral bands and converts image into a new color system that separates the spectral details from the spatial ones. Then, the component of MS, which is supposed to contain the most spatial information, is substituted by the PAN image. Finally, by applying the inverse of color transform, the fused image is achieved. Intensity hue saturation [6], Gram Schmidt [7], principal component analysis [8], Brovey transform [9], band dependent spatial details [10] and different versions of them [11]-[13] are among the most well known CS methods.

The MRA or MST approaches generally try to separate the low pass bands containing the approximate of image from the high pass bands containing the details of images through applying an image decomposition to source images (MS and PAN). Then, a fusion rule is used to combine the appropriate bands of source images. Finally, by applying the inverse of MST, the fused image is synthesized. In other words, it can be said that MRA approaches inject the high frequencies of PAN into the upsampled MS bands. Laplacian pyramid (LP) [14], ratio of low pass pyramid (RP) [15], discrete wavelet transform (DWT) [16], dual tree complex wavelet transform (DTCWT) [17], curvelet transform (CVT) [18], and nonsubsampled contourlet transform (NSCT) [19] are among the popular and state-of-the-art MST methods [20]. In addition to CS and MRA approaches, there are other types of approaches such as model based methods which consider a model such as Bayesian [21] or a data representation type such as sparse representation [22] for modeling of source images or fused image. Some other pansharpening approaches are the hybrid methods which use two or more CS, MRA or model based methods to provide the advantages of all of them [23]-[24]. Estimate of parameters in model based methods and policy of integration are the main challenges of the model based and hybrid methods, respectively. Moreover, they have burden complexity too. The pansharpening methods generally try

*Corresponding author's email: maryam.imani@modares.ac.ir

to provide a good compromise between spectral and spatial quality. The CS and MRA methods exhibit a complementary spatial-spectral quality trade off. The CS methods often can render the spatial details in the fused image with a high fidelity while they often result in significant spectral distortion. This distortion is due to that the PAN sensor does not exactly cover the same wavelengths as the MS sensor. Performing histogram matching of PAN to the selected component of MS before implementation of substitution can degrade the spectral distortion. The histogram-matched PAN image will have the same mean and variance of the replaced component. On the contrary, the MRA approaches can efficiently preserve spectral information but they often result in spatial distortions such as staircase or ringing effects. However, the better matching between the frequency response of low pass filter used in MST with the modulation transfer function (MTF) of the spectral channel which PAN details are injected to it decreases the spatial distortion [25].

The application of nonlinear decomposition methodology to the pansharpening field is studied in [26]. The proposed method utilizes the morphological half gradient operators to improve the quality of fusion product. The nonlinear decomposition algorithms based on mathematical morphological operators are used to implement the non-linear MRA methods. A detail discussion of morphological half-gradient as an extraction operator is given in [26]. Different versions of the decomposition approaches such as High-Pass Filtering (HPF), High Pass Modulation (HPM), the work of Laporterie-Déjean *et al.* [27] and Half Gradients (HG) by applying suggested morphological filters, called as MF-TO-HPF, MF-TO-HPM, MF-LA and MF-HG, respectively, have been discussed in [26].

Our main focus in this paper is on the MRA methods. To reduce the spatial distortions and redundant spatial features from the fused product, a method based on the morphological profile (MP) is introduced. The morphological operators can efficiently extract the geometrical structures and useful spatial information from the source MS and PAN images [28]-[29]. The proposed method well transforms the extracted features into the fused product. The closing by reconstruction operator can provide an approximate component of image. By duality, the opening by reconstruction operator can achieve a detail component of image. So, the closing and opening operators are applied to MS (band by band) and PAN images to provide good estimates of approximate and details images, respectively. In addition, a multi-scale approach is used which considers a range of different structuring element sizes that helps to explore a range of different spatial structures. The results obtained by different scales are eventually fused by using the max-absolute rule to find the final fused product. The proposed method is called as MP-MST where MP indicates the morphological profile while different transforms such as LP, RP, DWT, DTCWT, CVT and NSCT can be replaced by MST. The experimental results on three real datasets acquired by different sensors show the good quality of MP-MST compared to conventional MST in terms of several quality measures.

2- MULTI-SCALE TRANSFORMS

A) Laplacian pyramid (LP)

The LP transform generates a set of band pass copies of the given image. Due to similarity to the Laplacian operator, it is referred as the Laplacian pyramid. The LP transform can be implemented one dimensional (1D) or 2D. The 2D case is a straightforward extension of 1D. Generally, to implement a LP transform, a decimation filter is used to generate the low pass filtered version of input signal. Then, the filtered signal is downsampled to produce the coarse signal. To produce the detail signal, the coarse signal is upsampled and then, an interpolator filter is applied to obtain the prediction signal. The first level of the detail signal is achieved by subtracting the prediction signal from the original input one. This process is repeatedly applied to the coarse signal until the final resolution is achieved. Assuming the original $r_0 \times c_0$ image denoted by g_0 be the zero level or bottom of the pyramid. The image level 1 of pyramid is indicated by g_1 and is obtained by reducing and low pass filtering of g_0. Generally, we have: $g_l = reduce(g_{l-1}); 0 < l < N$ which means [14]:

$$g_l(i,j) = \sum_{a=-2}^{2}\sum_{b=-2}^{2} w(a,b)\, g_{l-1}(2i+a, 2j+b) \tag{1}$$

where N is the number of levels in the pyramid. The pixel in position (i,j) in image g_l is denoted by $g_l(i,j)$ where $0 < i < r_l$ and $0 < j < c_l$ and $r_l \times c_l$ is the size of g_l. The kernel $w(a,b) = w(a)w(b)$ is separable and symmetric. By considering $w(0) = m, w(-1) = w(1) = n$ and $w(-2) = w(2) = p$, it can be shown that three constraints $w(0) = m, w(-1) = w(1) = \frac{1}{4}$ and $w(-2) = w(2) = \frac{1}{4} - \frac{m}{2}$ are satisfied [30]. The shape of equivalent function is nearly similar to the Gaussian probability density function, and so, the sequence image $g_0, g_1, \ldots, g_N$ is called Gaussian pyramid. The Laplacian pyramid is also a sequence of differential images $L_0, L_1, \ldots, L_N$ which are the difference between two sequential levels of Gaussian pyramid. So, we have:

$$L_l = g_l - expand(g_{l+1}, 1) = g_l - g_{l+1,1}; 0 \le l \le N-1 \text{ and } L_N = g_N \tag{2}$$

which the *expand* operation is the inverse of *reduce* operation where generally $g_{l,k}$ is the image obtained by applying the *expand* operation to image g_l, k times, i.e., $g_{l,k} = expand(g_l, k-1)$, that means:

$$g_{l,k}(i,j) = 4\sum_{a=-2}^{2}\sum_{b=-2}^{2} w(a,b)\, g_{l,k-1}\left(\frac{i+a}{2}, \frac{j+b}{2}\right) \tag{3}$$

B) Ratio of low pass pyramid (RP)

In the LP transformed based fusion methods, each of source images is firstly transformed into a set of primitive pattern elements and then, the elements of various sources are combined to generate a single fused image where the fused image can be reconstructed from its primitive elements. Necessarily, the LP transform cannot be a good choice for image fusion [31]. The construction of RP transform is very similar to that of LP transform. Firstly, the Gaussian pyramid

of the input source image is generated. Then, instead of computing the difference image between the successive levels in the Gaussian pyramid (as the construction of LP), the ratio of two successive levels is taken. The result of this operation is referred to ratio of low pass (RP) which is defined by [15]:

$$R_l = g_l / expand\left(g_{l+1},1\right); 0 \le l \le N-1 \text{ and } R_N = g_N \quad (4)$$

So, the ratio of two successive layers in the Gaussian pyramid generates each level of RP. In the RP image fusion, the relative importance of pattern elements depends on their local luminance contrast values. So, the RP transform fits models of the human visual system. The visual system of human is sensitive to the local luminance contrast. In other words, the visually important details of images are presented in the fused image. For image fusion through RP transform, at first, the source images are decomposed into a set of dark and light blobs on different resolution levels. Then, the absolute contrast values of blobs at corresponding locations and at corresponding resolution levels are compared. Eventually, by selecting the blobs with the highest absolute value of luminance contrast, the image fusion is done and the fused image is generated by reconstruction from the set of blobs.

C) Discrete wavelet transform (DWT)

In the pyramid transform based image fusion method, the basic idea is to construct the pyramid transform of the composite (fused) image from the pyramid transforms of the source images. By taking the inverse pyramid transform, the fused image is generated. In the decomposition process, the pyramid transforms cannot introduce the spatial orientation selectively. So, they result in blocking effects in the fused images. Compared to pyramid transforms, DWT can provide better spectral and spatial localization of image information and causes lower color distortions. A wavelet is a waveform, a wave like oscillating, with limited duration and average value of zero. The wavelets are generally symmetric and irregular. A wavelet divides a given signal into different scale components. A 1D wavelet transform decomposes a signal with each level corresponding to a lower frequency band and a higher frequency band through applying the low pass filters and high pass filters followed by a downsampling, respectively. The signal is reconstructed through upsampling and applying the low and high synthesis filters. For implementation of a 2D DWT, a 1D DWT firstly is performed along the rows of image and then along the columns to generate 2D decomposition of image. The result is a set of approximation coefficients in addition to three sets of details coefficients where they are represent the horizontal, vertical and diagonal directions of images. In other words, four sub images corresponding to outputs of low-low, low-high, high-low and high-high bands are provided. A 2D DWT of a given image $f(x,y)$ with the size of $M \times N$ can be expressed by [32]:

$$F_\varphi\left(j_0,m,n\right) = \frac{1}{\sqrt{MN}} \sum_{x=0}^{M-1}\sum_{y=0}^{N-1} f\left(x,y\right)\varphi_{j_0,m,n}\left(x,y\right) \quad (5)$$

$$F_\psi^i\left(j,m,n\right) = \frac{1}{\sqrt{MN}} \sum_{x=0}^{M-1}\sum_{y=0}^{N-1} f\left(x,y\right)\psi_{j,m,n}^i\left(x,y\right); i = \{H,V,D\} \quad (6)$$

where

$$\varphi_{j,m,n}\left(x,y\right) = 2^{j/2}\varphi\left(2^j x - m, 2^j y - n\right) \quad (7)$$

$$\psi_{j,m,n}^i\left(x,y\right) = 2^{j/2}\psi^i\left(2^j x - m, 2^j y - n\right) \quad (8)$$

and index i indicates the directional wavelets. In addition, index i is a superscript that gives the values of horizontal (H), vertical (V) and diagonal (D). j_0 denotes an arbitrary scaling scale and $F_\varphi(j_0,m,n)$ coefficients provide an approximation of $f(x,y)$ at scale j_0. The $F_\psi^i(j,m,n)$ coefficients provide horizontal, vertical and diagonal details for scales $j \ge j_0$. Generally, j_0 is set as $j_0 = 0$ and $M = N = 2^j$, $j = 0,1,2,\ldots,j-1$ and $m = n = 0,1,2,\ldots,2^j - 1$.

For fusion of two source images using DWT, the images are decomposed into wavelet transformed images. Then, the transform coefficients of source images are fused based on a fusion rule. Finally, the fused image is generated by performing the inverse wavelet transform.

D) Dual tree complex wavelet transform (DTCWT)

DWT is an example of real valued wavelet transform whereas DTCWT is an example of complex wavelet transform. Although, the real valued wavelet transforms have better sparsely data representation and are computationally efficient; but, they suffer from shift variance, lack of directionality, absence of phase information, and aliasing. Shift variant means that a small change in the input signal results in a significant change in the energy distribution of wavelet coefficients at several levels of decomposition process. Downsampling in the decomposition process of DWT causes shift variance. DWT also suffers from lack of directionality because it supports just three directions of horizontal, vertical and diagonal. Many images contain edges oriented in random directions other than horizontal, vertical and diagonal. So, the real valued DWT may not be efficient for them. Phase information computed by both real and imaginary parts of complex valued signal, which gives the local behavior of a function, is absent in DWT. The downsampling operation which iteratively applied in the computation of real valued DWT causes aliasing that results in artifacts in the reconstructed image. To overcome to these problems, the complex wavelet transforms such as DTCWT have been introduced. DTCWT is implemented by using two real DWT in parallel where one of DWTs generates the real part and other one provides the imaginary part. Compared to DWT, DTCWT gives three sub images where each of them is in two quadrants, i.e., six sub images strongly oriented in the directions $\pm 15°, \pm 45°$ and $\pm 75°$ are provided. A 2D DTCWT can be defined by [17]:

$$\psi\left(x,y\right) = \psi\left(x\right)\psi\left(y\right) \quad (9)$$

where $\psi(x)$ and $\psi(y)$ denote two complex wavelets as follows [33]:

$$\psi(x)=\psi_h(x)+j\psi_g(x) \tag{10}$$

$$\psi(y)=\psi_h(y)+j\psi_g(y) \tag{11}$$

where $\psi_h(x)$ and $\psi_h(y)$ indicate the real wavelet transforms of upper and lower filter banks, respectively, and $\psi_g(x)$ and $\psi_g(y)$ are the corresponding complex parts. Then, we have:

$$\begin{aligned}\psi(x,y)&=\left[\psi_h(x)+j\psi_g(x)\right]\left[\psi_h(y)+j\psi_g(y)\right]\\&=\psi_h(x)\psi_h(y)-\psi_g(x)\psi_g(y)+\\&j\left[\psi_g(x)\psi_h(y)+\psi_h(x)\psi_g(y)\right]\end{aligned} \tag{12}$$

E) Curvelet transform (CVT)

The Fourier transform is not able to handle the point discontinuities since a discontinuity point affects all the Fourier coefficients. In contrast to Fourier transform, the wavelet transform can well handle the point singularities. But, it is not able to handle curve discontinuities. To deal with this problem, the curvelet transforms (CVTs) are introduced. They are designed for representation of curved shapes using a small number of coefficients. To implement a CVT, the image is decomposed into a set of sub-bands by using the wavelet transforms. Then, each subband is analyzed by utilizing a local ridgelet transform. Mathematically, it can be considered as a wavelet analysis in the radon domain. The radon transform is a facility for shape detection. So, the ridgelet transform is also useful for detection of ridges and shapes of objects in an image. The ridgelet transform can efficiently handle the line singularities. The aim is to map a line singularity in 2D domain into a point one by applying the radon transforms. Therefore, a 1D wavelet is implemented to handle the point singularities in the radon domain. The ridgelet basic function is given by [18]:

$$\psi_{a,b,\theta}=a^{-\frac{1}{2}}\psi\left(\frac{x_1\cos\theta+x_2\sin\theta-b}{a}\right) \tag{13}$$

and the ridgelet coefficients are computed as follows:

$$R_f(a,b,\theta)=\iint\psi_{a,b,\theta}(x_1,x_2)f(x_1,x_2)dx_1dx_2 \tag{14}$$

The ridgelet transform $R_f(a,b,\theta)$ can be represented in terms of radon transform $R_f(\theta,t)$ by:

$$R_f(a,b,\theta)=\int_{-\infty}^{\infty}R_f(\theta,t)a^{-\frac{1}{2}}\left(\frac{t-b}{a}\right)dt \tag{15}$$

where the angular variable θ is constant while t is varying and the radon transform of f, which is a collection of line integrals indexed by $(\theta,t)\in[0,2\pi)\times R$, is given as follows [34]:

$$R_f(\theta,t)=\int_{-\infty}^{\infty}\int_{-\infty}^{\infty}f(x_1,x_2)\delta(x_1\cos\theta+x_2\sin\theta-t)dx_1dx_2 \tag{16}$$

F) Nonsubsampled contourlet transform (NSCT)

NSCT is an example of overcomplete transform which is a shift invariant version of contourlet transform. Shift invariance, multi-direction and multi-scale are some good properties of NSCT in the process of image decomposition. An appropriate representation of contours is provided by NSCT. There are two main components in NSCT. The first is nonsubsampled pyramid filter bank structure for multi-scale decomposition. The second is a nonsubsampled directional filter bank structure for directional decomposition.

To implement NSCT for image fusion, there are some main steps. First, NSCT is applied to the source images to acquire low pass subband coefficients at each of scales and directions. The non-subsampled pyramid filter bank and the non-subsampled directional filter bank are used to provide the multi-scale decomposition and the multi-direction decomposition, respectively. In the second step, according to a given fusion rule, the transformed coefficients are combined to obtain the NSCT coefficients of the fused image. Finally, by performing the inverse NSCT to the selected coefficients obtained from the previous steps, the fused image is reconstructed.

3- PROPOSED METHOD

The proposed fusion method in this work utilizes the advantages of morphological operators for extraction of useful spatial structures from the source images. To this end, the closing operator is applied for extraction of local structures of the approximation image of MS and the opening operator is used for extraction of the sharp components, i.e., the details image, of PAN. The multi-scale structural elements (SEs) are used to provide a range of different SE sizes which result in appearance of spatial structures with different sizes in the final product. Before detail description of the proposed method, a brief review of morphological operators and their properties is given in the following, and then, the proposed fusion method is described.

A) Morphological operators and properties

The morphological filters can effectively extract appropriate features for modeling the spatial information of images. The basic operators in mathematical morphology are erosion and dilation where these operators are applied to a given image with a set of known shape called as SE. Applying the erosion operator to an image results in an output image that shows where SE fits the objects present in the images. In contrast, applying the dilation operator to an image provides an output image that shows where SE hits the objects present in the image. These operations are dual and other morphological operators can be expressed in terms of them. The opening and closing operators are two popular morphological operators where opening means to dilate an eroded image while closing

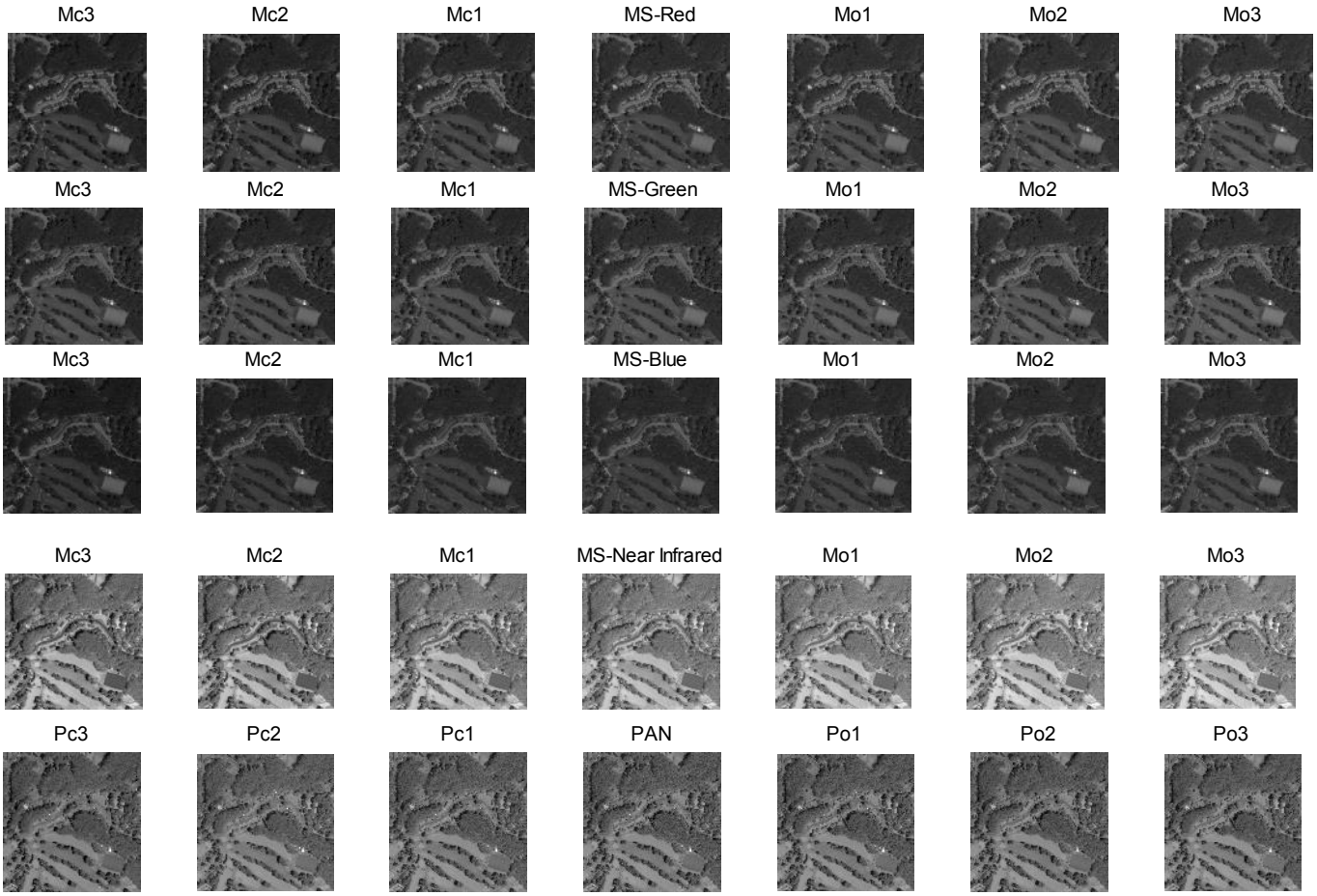

Fig. 1. Three closing and three opening components of MS bands (Red, Green, blue and near infrared) and PAN image for GeoEye dataset.

means to erode a dilated image.

The opening and closing operators should be implemented by using a non-Euclidean metric, known as filtering by reconstruction. The family of operators by reconstruction can better preserve shapes than the classical morphological operators. The reason is that the shape of SE used in the filtering by reconstruction is adaptive with respect to the structures present in the image. An opening by reconstruction operator removes from a scalar image all those bright connected components that the SE does not fit in. Bright components mean the brighter components with respect to grey levels of neighboring regions. The opening operator does not distort the edges of regions. It just

merges the flat regions while preserves the geometrical characteristics of the structures which do not remove from the image. By duality, a closing by reconstruction operator removes the dark connected components from the image. The opening γ and closing φ by reconstruction filter outputs of a grey level image f are defined, respectively as follows [35]:

$$\gamma_R^i(f) = R_f^\delta\left(\varepsilon^i(f)\right) \tag{17}$$

$$\varphi_R^i(f) = R_f^\varepsilon\left(\delta^i(f)\right) \tag{18}$$

where ε^i and δ^i denote the erosion and dilation operators with a SE of size i, respectively and R_f^δ and R_f^ε indicate the geodesic reconstruction by dilation and erosion, respectively.

B) MP-MST fusion method

By applying the opening operators, the details of image are enlarged. In other words, more details of image are appeared in the opening components of an image. In contrast, by applying the closing operators, the spatial details have more tendency to become similar to the neighboring regions. We can use these useful characteristics of opening and closing operators for extraction of appropriate features from MS and PAN images. The closing and opening components of four bands of MS image (red, green, blue and near infrared) and also the PAN image of GeoEye dataset are shown in Fig. 1.

The aim of pansharpening is to fuse the MS and PAN images to provide a fused image with both high spatial resolution of PAN and high spectral resolution of MS. In other words, we want to integrate the approximate information of MS with the details information of PAN to achieve the fused product. The MST methods are used for fusion of MS and PAN images in this paper. But, to highlight the main characteristics of MS and PAN images in the fusion process, the morphological operators by reconstruction are used. To decrease the redundant spatial details and noise from the MS

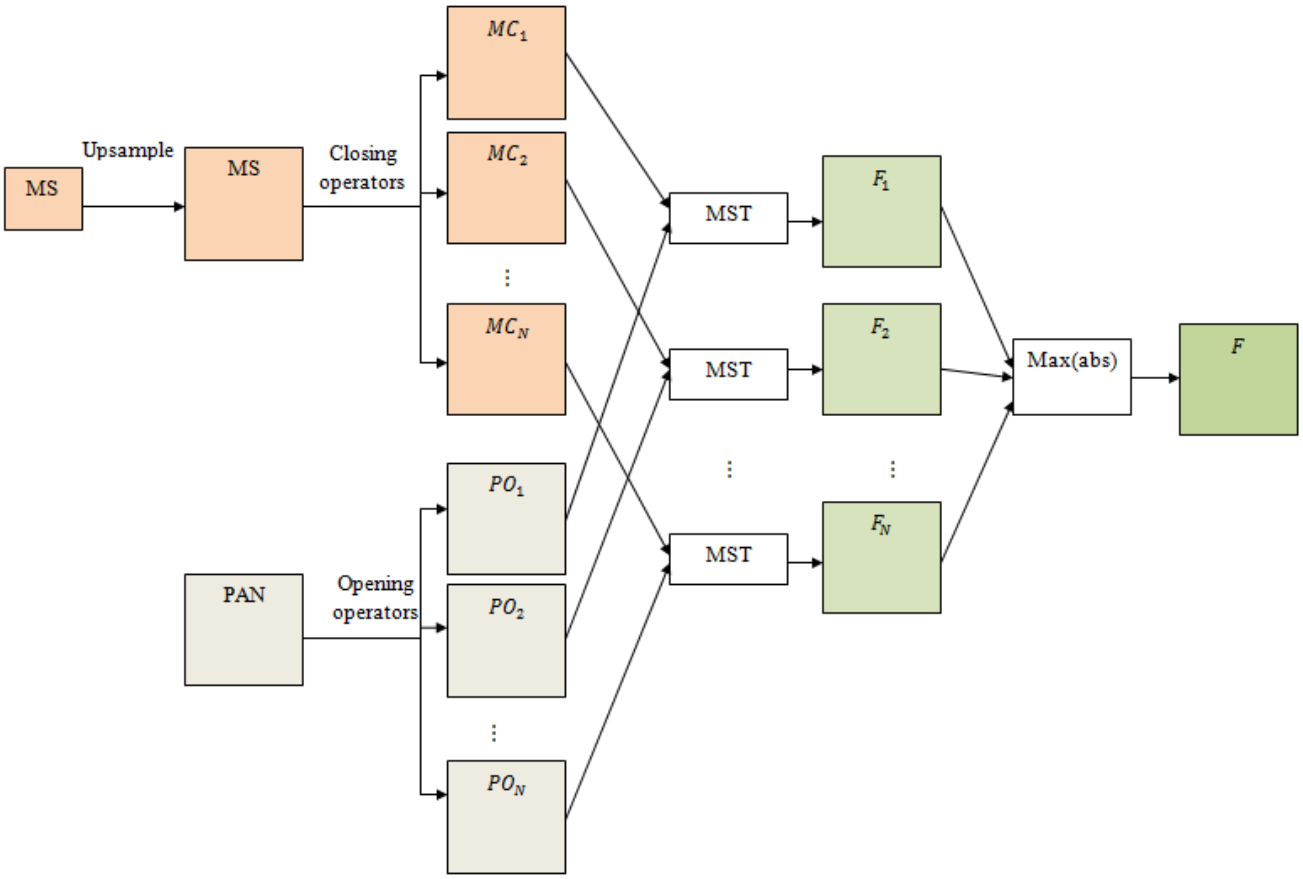

Fig. 2. Bock diagram of the proposed MP-MST fusion method (the fusion of MS with PAN is done band by band. For simplicity, the subscript related to band k of MS is omitted.

image, the closing by reconstruction operator is applied to the MS image. In contrast, to highlight the useful spatial details of PAN, the opening by reconstruction operator is applied to the PAN image.

Some spatial structures present in the image may have a high response for a special SE size and a lower response for other SE sizes depending on the interaction between the size of spatial structure and the SE size. So, to explore the spatial information of various structures with different sizes, it is appropriate to use a multi-scale approach based on a range of different SE sizes. This idea helps to utilize the best response of the structures in the image. The block diagram of the proposed fusion method is shown in Fig. 2. The MS image is fused with the PAN image band by band. Fig. 2 shows the fusion process of a band of MS with PAN. To fuse each band of MS with PAN, at first the MS image is upsampled to be as the same size of PAN. Then, N closing by reconstruction operators are applied to MS to provide N closing components of MS denoted by MC_1, MC_2, …, MC_N. In duality, N opening by reconstruction operators are applied to PAN to provide N opening components of PAN denoted by PO_1, PO_2, …, PO_N. Each corresponding pair of closing components of MS and opening components of PAN are fused together using a MST method. In other words, MC_1 and PO_1 are fused to obtain F_1; MC_2 and PO_2 are fused to provide F_2, and so on. The final fused product F is obtained from the $F_1, F_2, \ldots, F_N$ images by applying the maximum absolute (max(abs)) rule. In other words, in each pixel position, the value of $F_i; i = 1,2,\ldots,N$ with the largest absolute value is chosen as the pixel value of the fused image F.

In this paper, different MST methods are used to evaluate the performance of the proposed fusion method: LP, RP, DWT, DTCWT, CVT and NSCT. The proposed method is general is indicated by MP-MST where the names of different MST approaches can be replaced by MST, i.e., MP-LP, MP-RP, MP-DWT, MP-DTCWT, MP-CVT and MP-NSCT. Some advantages of the proposed fusion method are presented in the following:

1) By applying the morphological filters to the source images before MST, useful local spatial features are extracted. Moreover, the noise and redundant spatial details which may cause local artifacts in the fused product is decreased.

2) The closing operator can provide a suitable approximation image of MS while the opening operator can achieve an appropriate detail image of PAN. The fuse of closing based transformed MS and opening based transformed PAN can provide a fused product with improved quality than the fuse of original MS and PAN images.

3) By applying several closing and opening operators with different SE sizes, various structures with different sizes depending on the size of objects present in the image can

be extracted. The use of max(abs) rule for integrating the information of different scales can provide the fused image with more spectral and spatial information with respect to the single scale with just a SE size.

4- EXPERIMENTS

The performance of the proposed fusion method, which is generally called MP-MST, is compared to widely used MST methods. Six different MST approaches, i.e., LP, RP, DWT, DTCWT, CVT and NSCT are assessed in this paper. The performance of MP-LP, MP-RP, MP-DWT, MP-DTCWT, MP-CVT and MP-NSCT is compared to MST themselves.

A) Datasets and quality measures

Three MS and PAN image sources acquired by different remote sensors, GeoEye, QuickBird and IKONOS are used for doing experiments. The sizes of used MS and PAN images are 256×256 pixels and 1024×1024 pixels, respectively. The experimented MS images in GeoEye and IKONOS datasets consist of four bands of red, green, blue and near infrared while MS in the used QuickBird dataset has three bands. The MS and PAN images have the spatial resolution of.46 m and 1.84 m, respectively in GeoEye. In IKONOS, the spatial resolution of MS and PAN images are 0.82 m and 3.2 m, respectively and in QuickBird, the PAN image has 0.65 m pixel resolution.

Due to the lack of high resolution (HR) MS image, i.e., the fused product, as the reference image, the quantative evaluation of fusion results is an open and challenging problem. One of the most practical protocols to deal with this problem has been proposed by Wald [36]. This protocol uses the original HR image as the reference image. It degrades the original MS and PAN images with a scale equal to the ratio between scales of MS and PAN. The degraded MS and PAN images are fused to provide a HR MS image with the same scale of the original MS. Then, the fused product is compared to the original MS image as the reference. The Wald's protocol utilizes two main properties: consistency and synthesis. The consistency property means that the original MS image should be achieved by simply degrading the fused image. The synthesis property states that the pansharpened image has to reproduce characteristics of the original MS image at a higher resolution.

Different quality indices are used to evaluate the performance of the proposed methods compared to others: root mean square error (RMSE), spectral angle mapper (SAM), degree of distortion (D), error relative dimensionless global error in synthesis (ERGAS), correlation coefficient (ρ), and universal image quality index (UIQI). In addition, a non-reference quality metric called feature mutual information (FMI) is used to assess the quality of fused products without considering the reference images [37]. The concept of information contained in an image is represented by its features. The amount of information of these features conducted from the source images (MS and PAN) to the fused product (pansharpened image) can be a desirable criterion to evaluate the performance of the fusion methods. The mutual information measures the similarity of two variables and shows the amount of information that a random variable has about another. By considering x and y as two random variables, the degree of dependency between them is measured by Kullback-Leibler relation:

$$I(x,y)=\sum_{x,y}p(x,y)\log_2\frac{p(x,y)}{p(x)\,p(y)} \tag{19}$$

where $p(x,y)$ is the joint probability distribution function (joint PDF) while $p(x)$ and $p(y)$ are the marginal PDFs. Assuming A and B be the source images and F is the fused image. To obtain the FMI metric, at first, a feature extraction method is used to extract the feature image of the source images and the fused image [38]. Each desirable feature extractor can be used. As proposed in [37], the gradient is chosen. The gradient map contains useful information about contrast, texture, edges, pixel neighborhood and directions. After applying the feature extraction transform, the feature images are normalized to obtain the marginal PDFs $p(a)$, $p(b)$, and $p(f)$. To decrease the computational burden, small corresponding slide windows between the fused and source images are used to measure the regional FMI. The FMI metric between the source images A and B and the fused image F can be obtained by:

$$FMI_F^{A,B}=\frac{1}{n}\sum_{i=1}^{n}\left(\frac{I_i(A;F)}{H_i(A)+H_i(F)}+\frac{I_i(B;F)}{H_i(B)+H_i(F)}\right) \tag{20}$$

where $n=M\times N$ that $M\times N$ is the size of image. $I_i(A;F)$ is the mutual information between images A and F for ith slide window. Similarly, $I_i(B;F)$ is the mutual information between images B and F. $H_i(A)$, $H_i(B)$ and $H_i(F)$ are the entropies of the corresponding windows from images A, B and F.

B) Assessment of pansharpening results

One of the free parameters, which has to be set in MST methods, is the decomposition level. From one hand, to provide enough spatial details from the source images, the decomposition level should not be small. From the other hand, a large decomposition level causes that a coefficient in the low pass component has an impact on a large number of pixels in the fused product. So, if there is an error in the low pass band due to noise or mis-registration between given source images, serious artifical effects are appeared in the fused image. In addition, in the MST with a large decomposition level, the fusion quality of high pass bands is also sensitive to mis-registration and noise. If the source images are not registered precisely due to different imaging parameters, choosing a large decomposition level is not reasonable.

In the proposed MP-MST fusion method, the rich spatial information of local structures with different sizes are provided by applying the opening and closing by reconstruction operators. So, even with choosing a small decomposition level, enough spatial features are provided from source

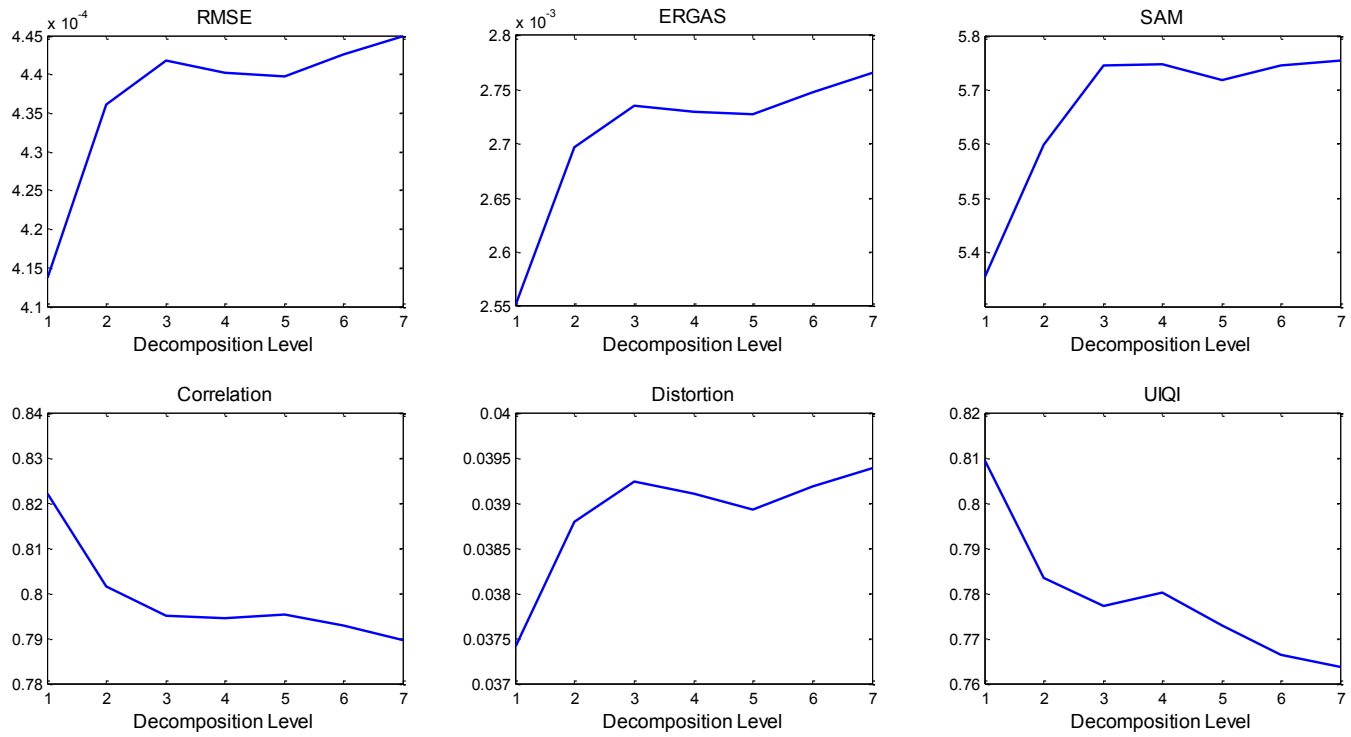

Fig. 3. Effects of decomposition level on the quality of fusion image in the MP-LP method.

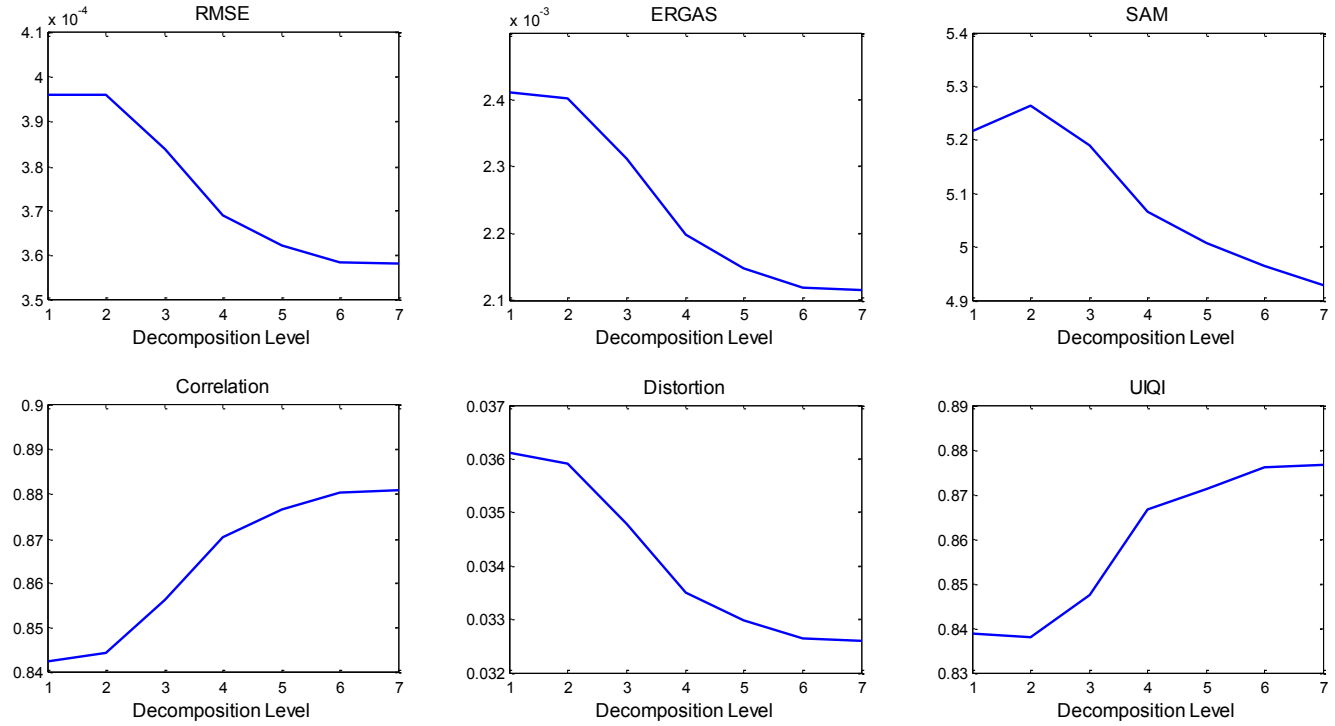

Fig. 4. Effects of decomposition level on the quality of fusion image in the MP-RP method.

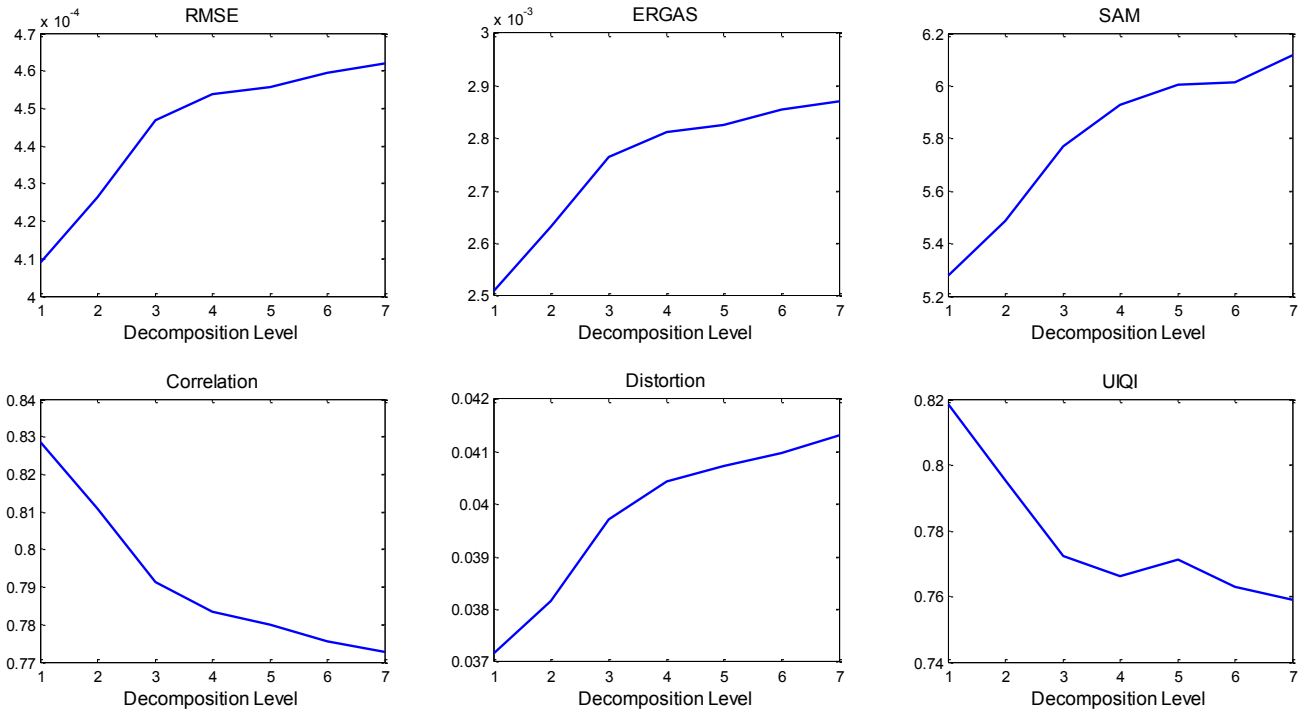

Fig. 5. Effects of decomposition level on the quality of fusion image in the MP-DWT method.

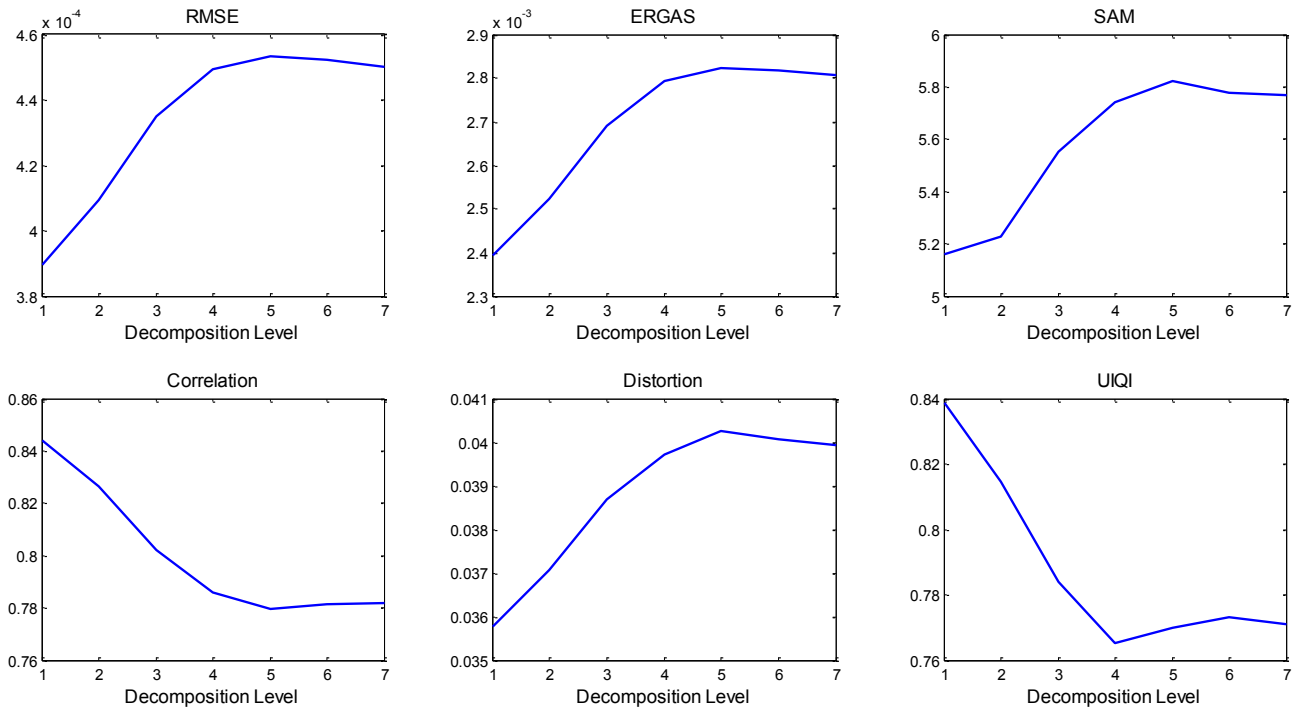

Fig. 6. Effects of decomposition level on the quality of fusion image in the MP-DTCWT method.

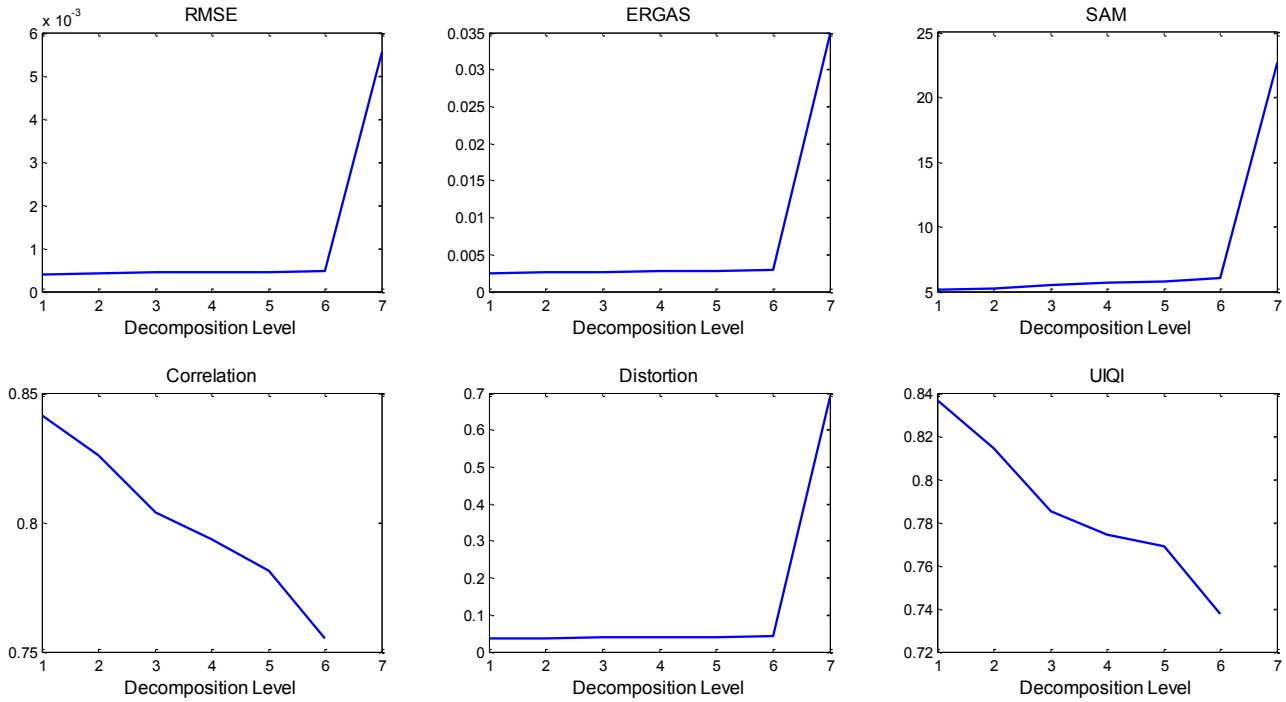

Fig. 7. Effects of decomposition level on the quality of fusion image in the MP-CVT method.

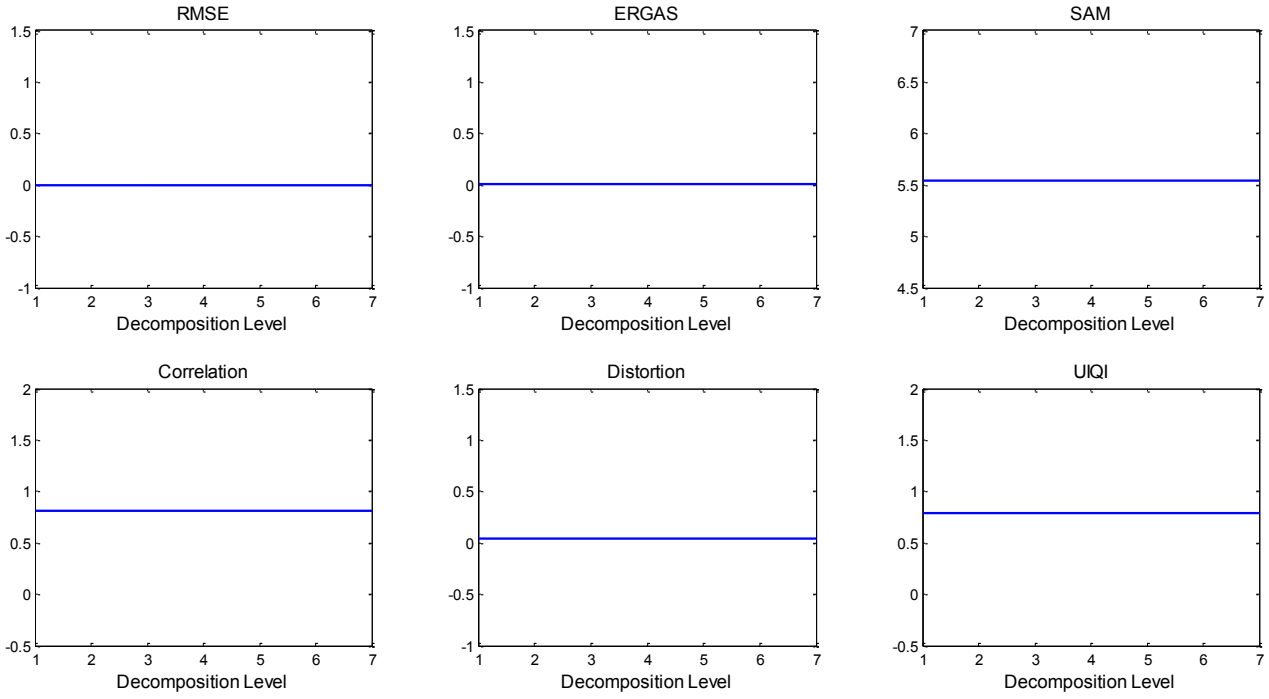

Fig. 8. Effects of decomposition level on the quality of fusion image in the MP-NSCT method.

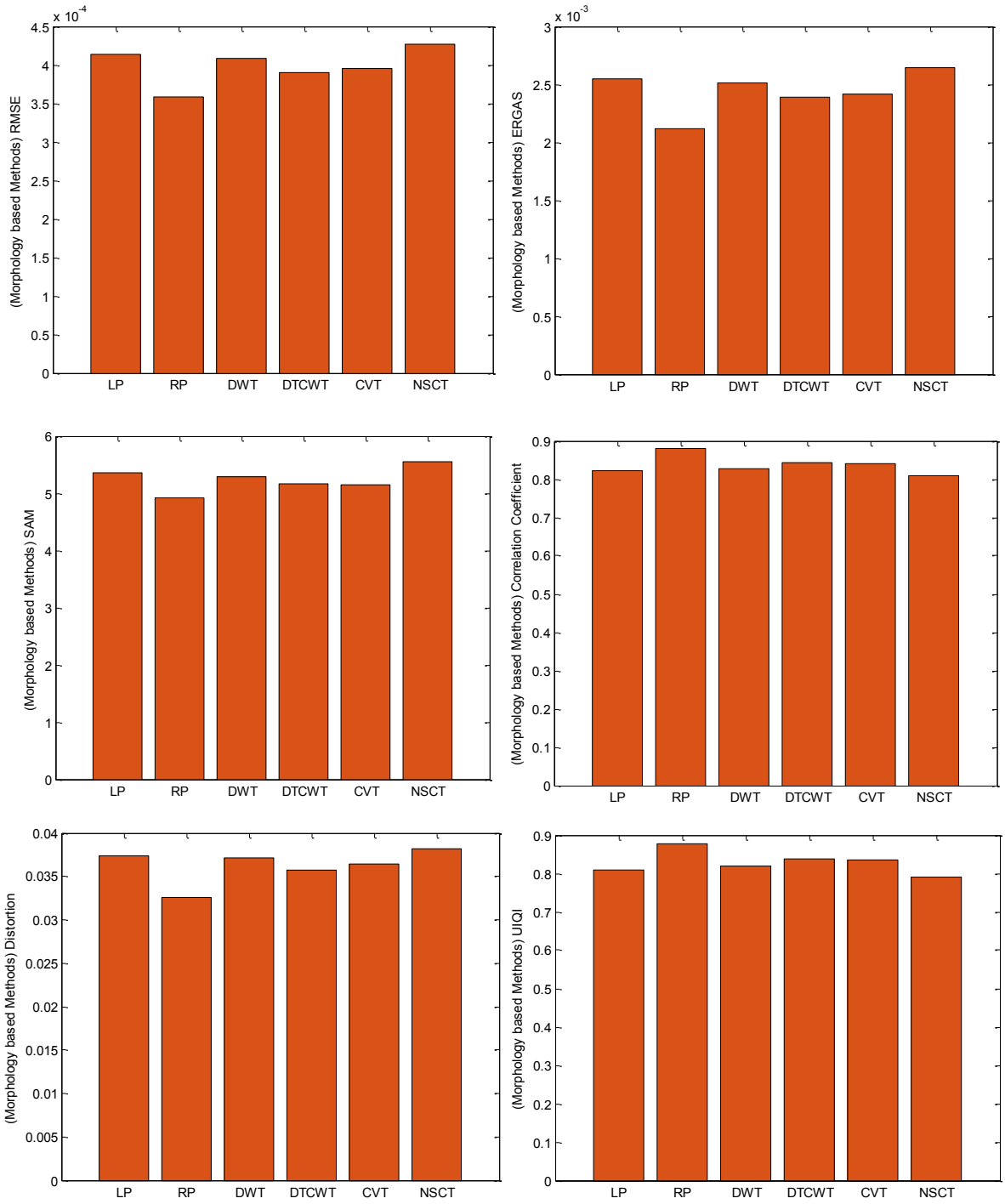

Fig. 9. Comparison between MP-MST methods in terms of RMSE, ERGAS, SAM, correlation coefficient, distortion and UIQI.

images. Therefore, a small decomposition level can be a good choice in MP-MST to avoid the artifical effects due to mis-registration between MS and PAN images. The quality of fusion image versus the decomposition level in terms of six quality measures for GeoEye dataset are shown in Figs. 3-8 for MP-LP, MP-RP, MP-DWT, MP-DTCWT, MP-CVT and MP-NSCT, respectively. According to the experimental results, the best performance is obtained by a decomposition level of 1 for MP-LP, MP-DWT, MP-DTCWT and MP-CVT while the best quality measures for MP-RP is provided by a decomposition level of 7. The experiments show that MP-NSCT has no sensitivity to the decomposition level.

The comparison between six proposed methods in terms of RMSE, ERGAS, SAM, correlation coefficient (ρ), distortion (D) and UIQI are shown in Fig. 9 for GeoEye dataset. The experiments show that MP-RP and MP-DTCWT can provide the best fusion results. The numerical comparison between the conventional MST methods and the proposed MP-MST ones are shown in Tables 1-3 for GeoEye, QuickBird and IKONOS datasets, respectively. The first column of each table

Table 1. Numerical results of the conventional MST methods and the proposed MP-MST methods for GeoEye dataset.

	Optimum values	LP	RP	DWT	DTCWT	CVT	NSCT	MP-LP	MP-RP	MP-DWT	MP-DTCWT	MP-CVT	MP-NSCT
RMSE	0	**0.0004**	**0.0004**	**0.0004**	**0.0004**	**0.0004**	**0.0004**	**0.0004**	**0.0004**	**0.0004**	**0.0004**	**0.0004**	**0.0004**
ERGAS	0	0.0027	0.0022	0.0026	0.0025	0.0025	0.0027	0.0026	**0.0021**	0.0025	0.0024	0.0024	0.0026
SAM	0	5.4097	**4.8874**	5.3141	5.1783	5.1627	5.5948	5.3547	4.9289	5.2809	5.1606	5.1505	5.5449
ρ	1	0.8081	0.8737	0.8196	0.8365	0.8343	0.7978	0.8221	**0.8810**	0.8285	0.8442	0.8413	0.8083
D	0	0.0390	0.0337	0.0383	0.0367	0.0373	0.0395	0.0374	**0.0326**	0.0372	0.0358	0.0364	0.0381
UIQI	1	0.7814	0.8648	0.8005	0.8235	0.8233	0.7663	0.8093	**0.8767**	0.8185	0.8386	0.8363	0.7904

Table 2. Numerical results of the conventional MST methods and the proposed MP-MST methods for QuickBird dataset.

	Optimum values	LP	RP	DWT	DTCWT	CVT	NSCT	MP-LP	MP-RP	MP-DWT	MP-DTCWT	MP-CVT	MP-NSCT
RMSE	0	0.0010	0.0010	0.0009	0.0009	0.0009	0.0010	0.0009	0.0009	0.0009	**0.0008**	**0.0008**	0.0009
ERGAS	0	0.0059	0.0057	0.0056	0.0054	0.0054	0.0062	0.0053	0.0054	0.0052	**0.0049**	0.0050	0.0056
SAM	0	5.8817	5.8375	5.7118	5.6468	5.6305	6.0021	5.7990	5.7772	5.6641	5.5504	**5.5358**	5.9866
ρ	1	0.7431	0.7758	0.7687	0.7865	0.7868	0.7153	0.7881	0.7949	0.8032	**0.8185**	0.8180	0.7645
D	0	0.0993	0.0934	0.0951	0.0923	0.0925	0.1038	0.0937	0.0897	0.0901	**0.0875**	0.0876	0.0978
UIQI	1	0.7401	0.7637	0.7674	0.7859	0.7863	0.7101	0.7874	0.7782	0.8024	**0.8171**	0.8165	0.7640

Table 3. Numerical results of the conventional MST methods and the proposed MP-MST methods for IKONOS dataset.

	Optimum values	LP	RP	DWT	DTCWT	CVT	NSCT	MP-LP	MP-RP	MP-DWT	MP-DTCWT	MP-CVT	MP-NSCT
RMSE	0	0.0005	0.0005	0.0005	0.0005	0.0005	0.0005	0.0005	0.0005	0.0005	**0.0004**	0.0005	0.0005
ERGAS	0	0.0026	0.0025	0.0025	0.0023	0.0024	0.0026	0.0024	0.0024	0.0024	**0.0022**	0.0023	0.0025
SAM	0	5.5583	5.3657	5.3835	5.2151	5.2229	5.6525	5.3981	5.2555	5.2453	**5.0894**	5.0906	5.4993
ρ	1	0.8811	0.8846	0.8888	0.9010	0.8968	0.8775	0.8945	0.8930	0.8979	**0.9088**	0.9051	0.8903
D	0	0.0498	0.0472	0.0481	0.0458	0.0468	0.0499	0.0470	0.0454	0.0461	**0.0441**	0.0450	0.0473
UIQI	1	0.8689	0.8748	0.8791	0.8917	0.8877	0.8646	0.8800	0.8839	0.8859	**0.8963**	0.8934	0.8757

represents the name of quality indices and the second column shows the optimum values of them. The best obtained quality index in each row of table is shown in bold.

In the GeoEye dataset, all methods have the same performance from the RMSE measure view point. In terms of other quality indices except SAM, the proposed MP-RP acquires the best results while the conventional version of it, i.e., RP provides the best value of SAM index. However, the SAM value of MP-RP is close to RP. In terms of ERGAS, after the MP-RP and RP methods, MP-DTCWT and MP-CVT are the best choices. The best values of correlation coefficient (ρ), distortion (D) and UIQI are provided by MP-RP, conventional RP and then, MP-DTCWT. With a comparison between LP and MP-LP, RP and MP-RP, DWT and MP-DWT, DTCWT and MP-DTCWT, CVT and MP-CVT, NSCT and MP-NSCT, it can be found that generally the MP-MST methods can provide better results than the MST methods.

In the QuickBird dataset, the best RMSE is obtained by MP-DTCWT and MP-CVT. The best SAM index is acquired by MP-CVT, and in terms of other quality indices, i.e., ERGAS, ρ, D, and UIQI, MP-DTCWT is the best fusion method. Generally, after MP-DTCWT, MP-CVT can be the best choice for pansharpening in QuickBird data. Similarly, in IKNOS dataset, MP-DTCWT and MP-CVT rank first and second, respectively.

The visual inspection of different fusion methods are shown in Figs. 10-12 for GeoEye, QuickBird and IKONOS datasets, respectively. As indicated in these figures, the main disadvantage of MST methods is appearance of noise and redundant spatial information in the pansharpened images while this problem is significantly solved in the MP-MST methods. The proposed MP-MST methods due to applying the morphological by reconstruction filters reduce the complexity of image while preserve the geometrical characteristics of local structures.

To better show the pixel difference between each reference (HR MS) image and the pansharpened image, the absolute value of difference of pixel values between the fusion image and the reference image is computed and shown for GeoEye, QuickBird and IKONOS datasets in Figs. 13-15, respectively. The difference value is calculated for each band and then, summed together to provide the total difference. In the error images, in Figs. 13-15, brighter and heater colors mean higher difference while darker and colder colors are corresponding to a small difference between the pansharpened product and the reference image. In GeoEye dataset, the smallest color

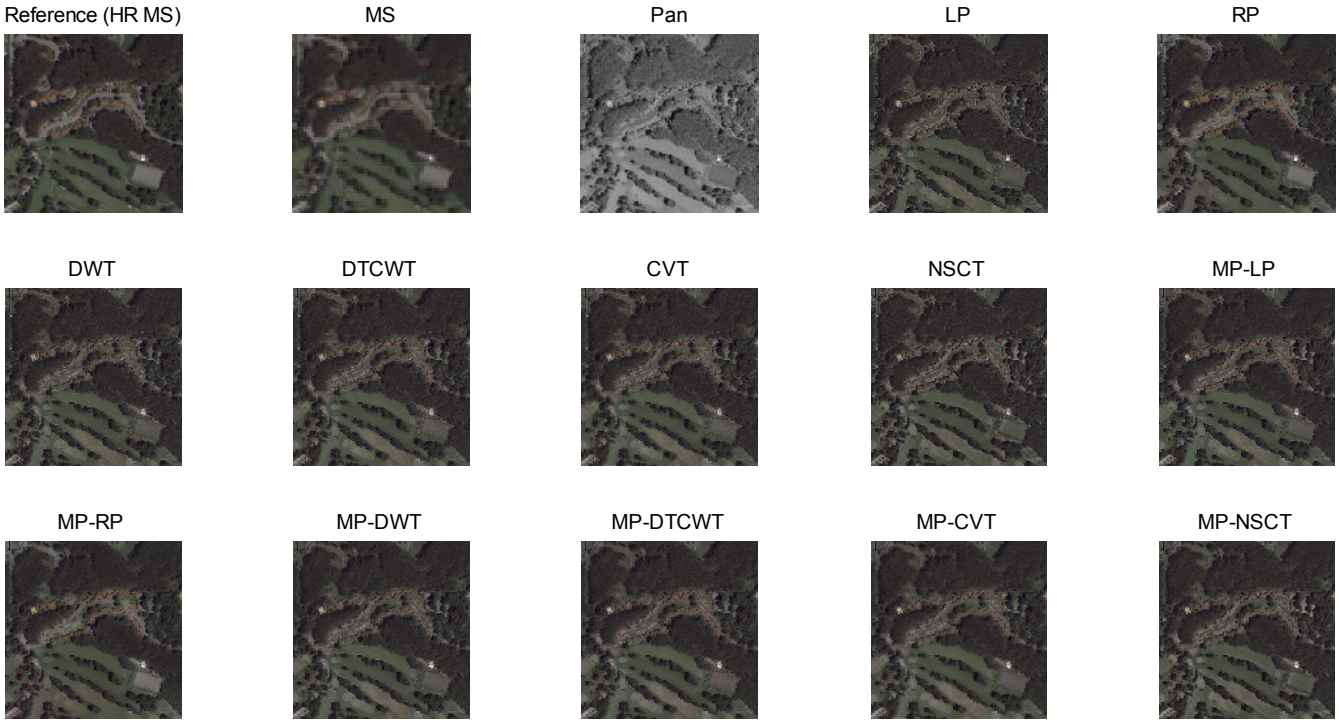

Fig. 10. Visual inspection of different fusion methods for GeoEye dataset.

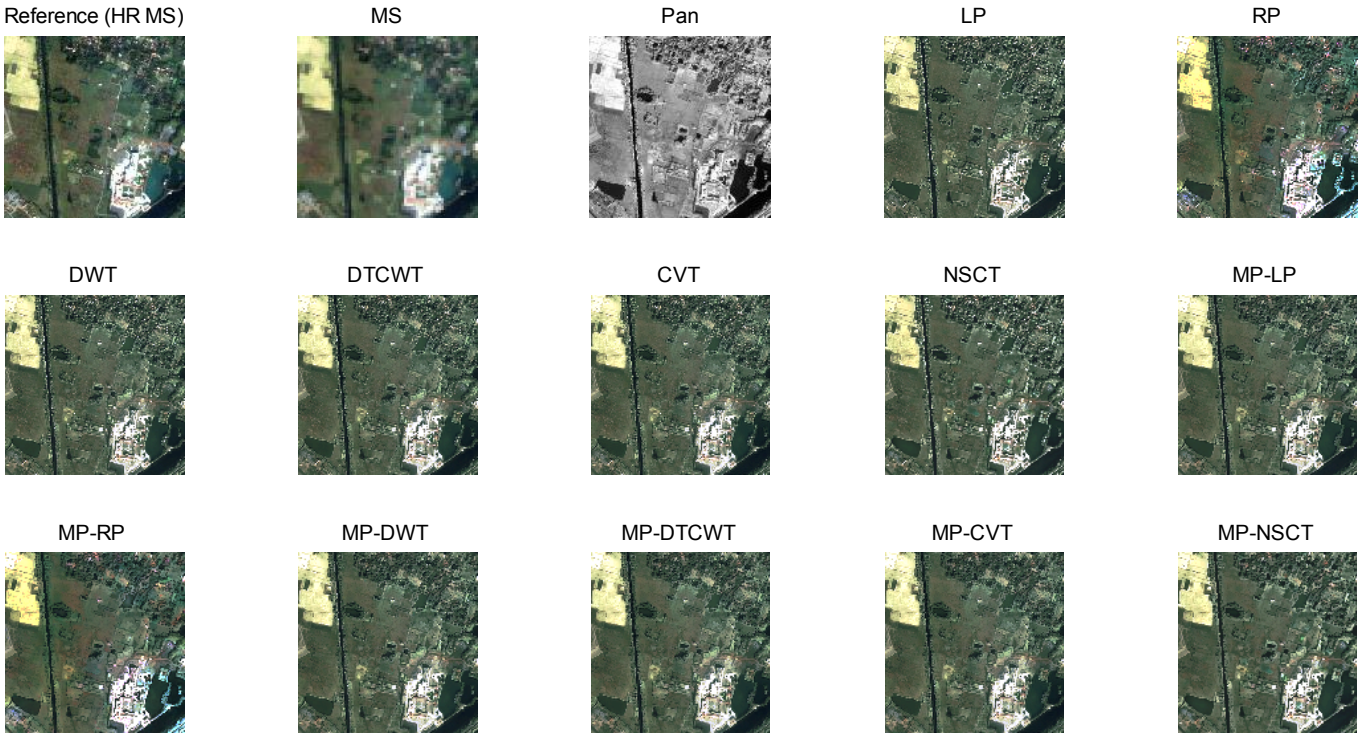

Fig. 11. Visual inspection of different fusion methods for QuickBird dataset.

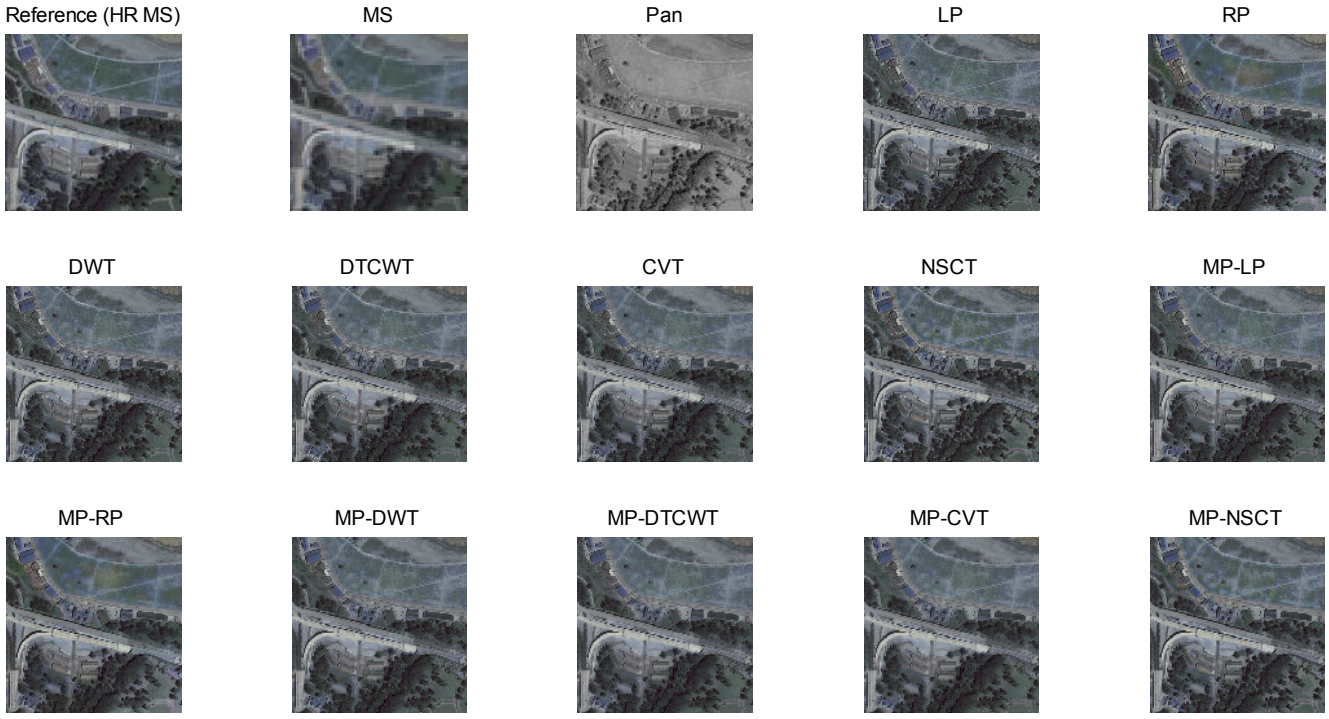

Fig. 12. Visual inspection of different fusion methods for IKONOS dataset.

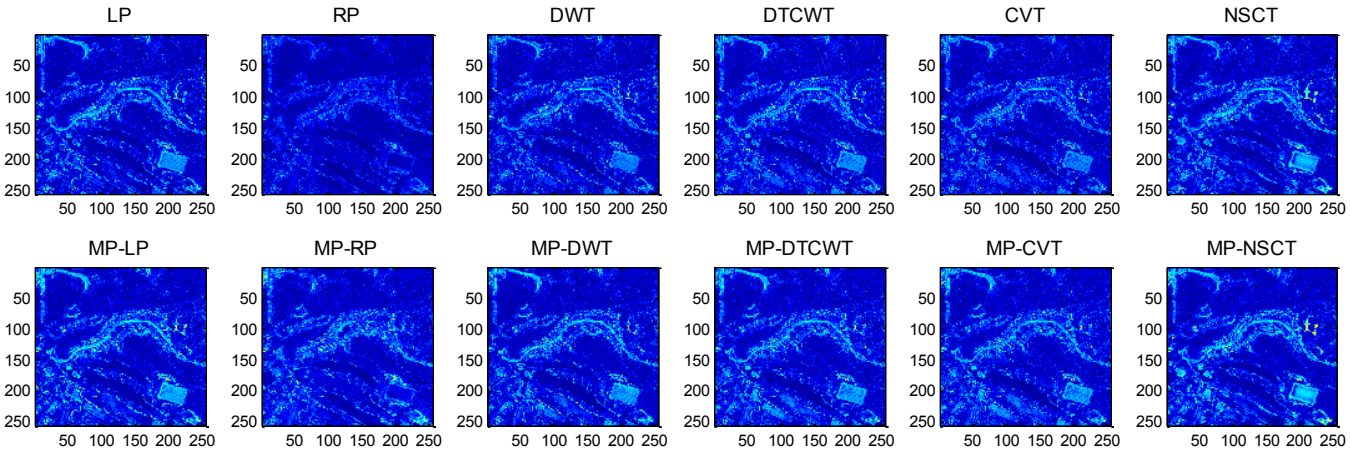

Fig. 13. Error images of different fusion methods for GeoEye dataset.

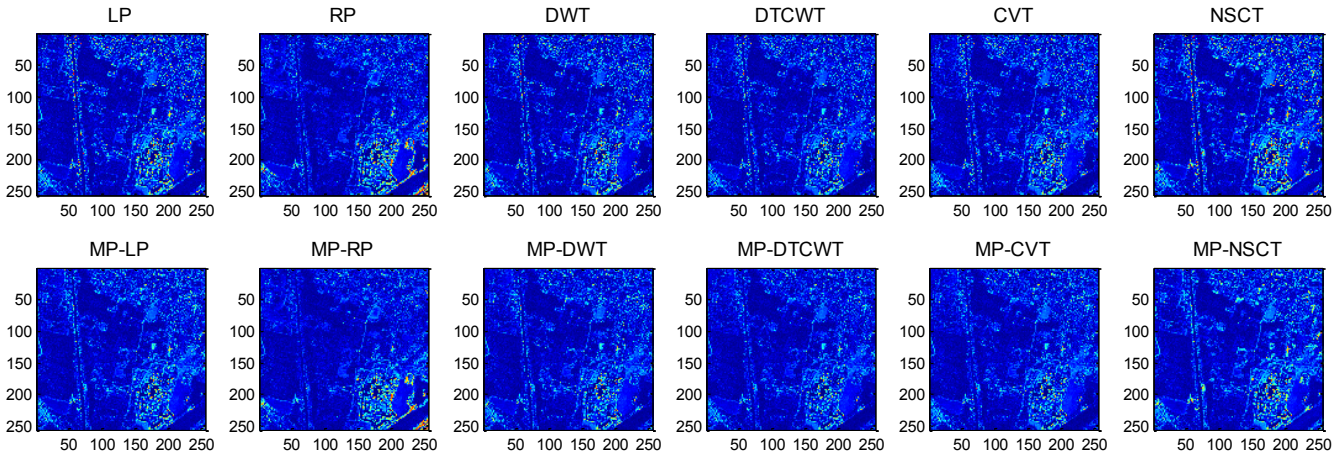

Fig. 14. Error images of different fusion methods for QuickBird dataset.

distortion is related to RP while LP, MP-LP, NSCT and MP-NSCT are related to the most color distortion. In QuickBird dataset, the smallest color distortion is obtained by MP-DTCWT and MP-CVT. In IKONOS dataset, MP-DTCWT and MP-CVT result in the smallest color distortion, respectively while RP and MP-RP cause more color distortions compared to other methods.

To assess the amount of spatial features, which can be either informative or redundant, the gradient energy maps are calculated for GeoEye, QuickBird and IKONOS datasets and shown in Figs. 16-18, respectively. The gradient energy maps are also shown for the HR MS, MS and PAN images. The gradient energies of different methods for three datasets are reported in Tables 4-6. As expected, the PAN image contains the most gradient energy and MS contains the smallest value. The HR MS, which is the reference image related to the fusion result of MS and PAN, has a gradient energy value between MS band PAN images. The obtained results show that generally MST methods have more gradient energy values compared to MP-MST ones. This is expected because the MP-MST methods by applying the morphological by reconstruction filters to the source images, i.e., MS and PAN, reduce the spatial

redundant features and noise from the fused product. Among the MST methods, RP contains the smallest gradient energy value in all datasets. DWT contains the largest gradient energy value in GeoEye and NSCT contains the largest gradient energy value in QuickBird and IKONOS datasets.

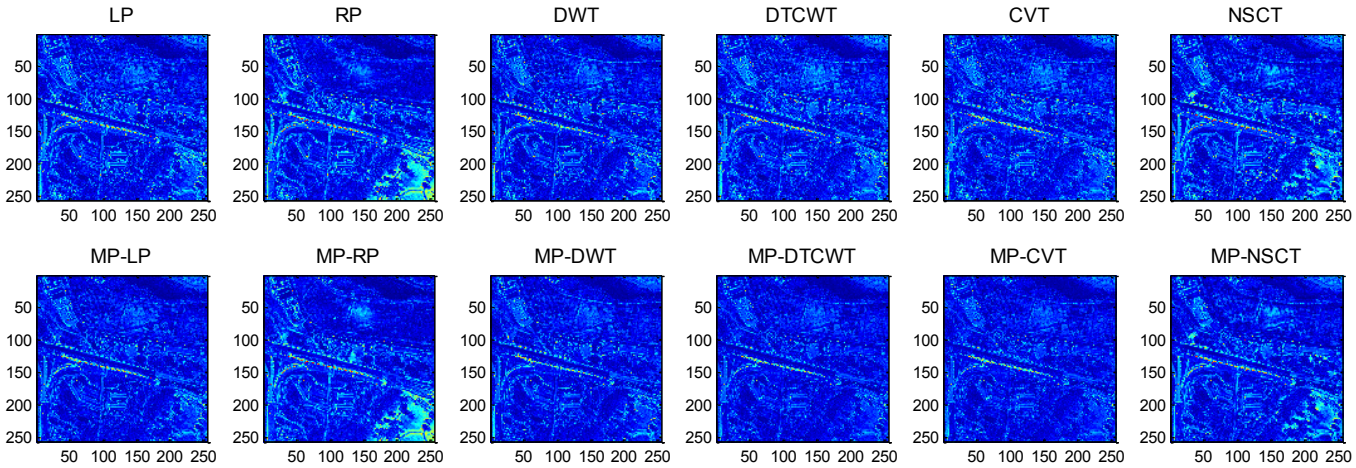

Fig. 15. Error images of different fusion methods for IKONOS dataset.

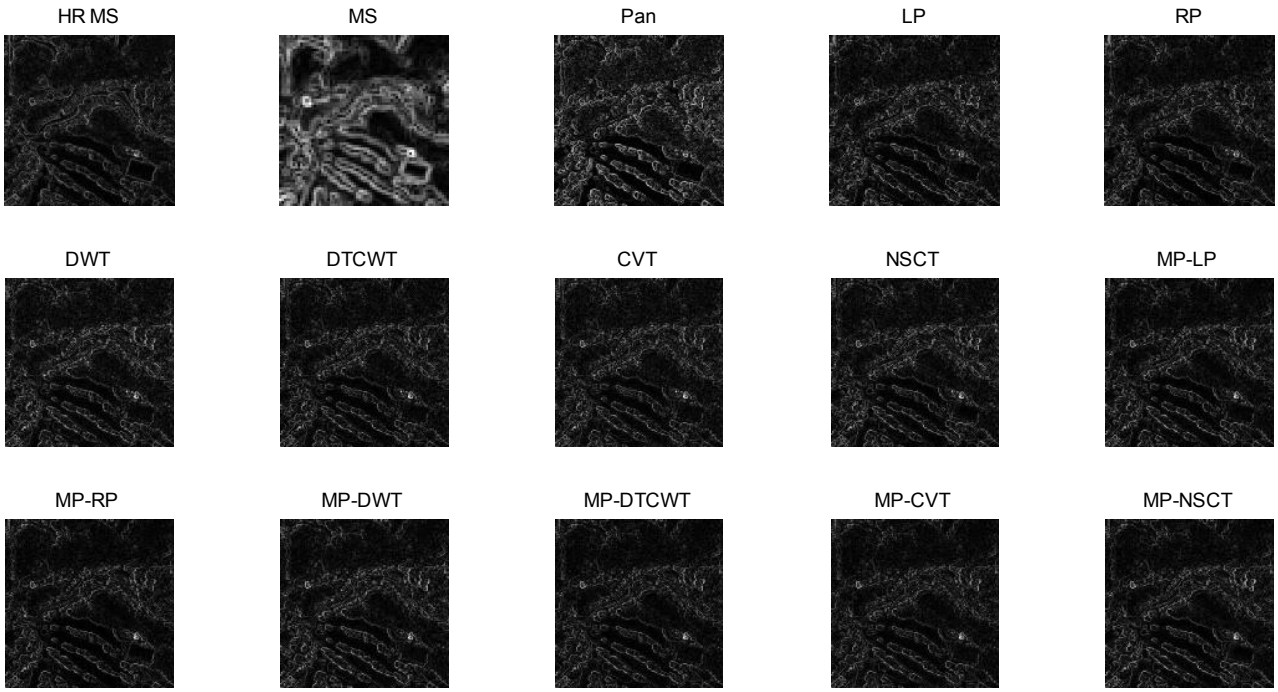

Fig. 16. Gradient energy maps of different fusion methods for GeoEye dataset.

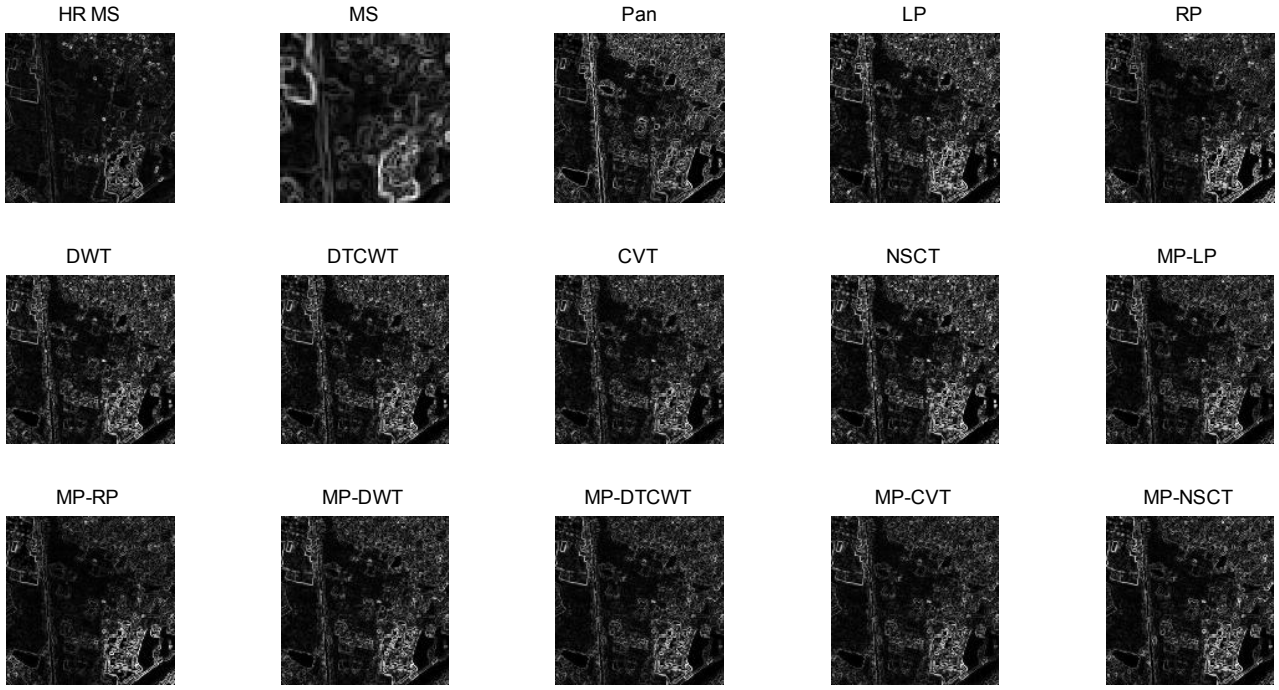

Fig. 17. Gradient energy maps of different fusion methods for QuickBird dataset.

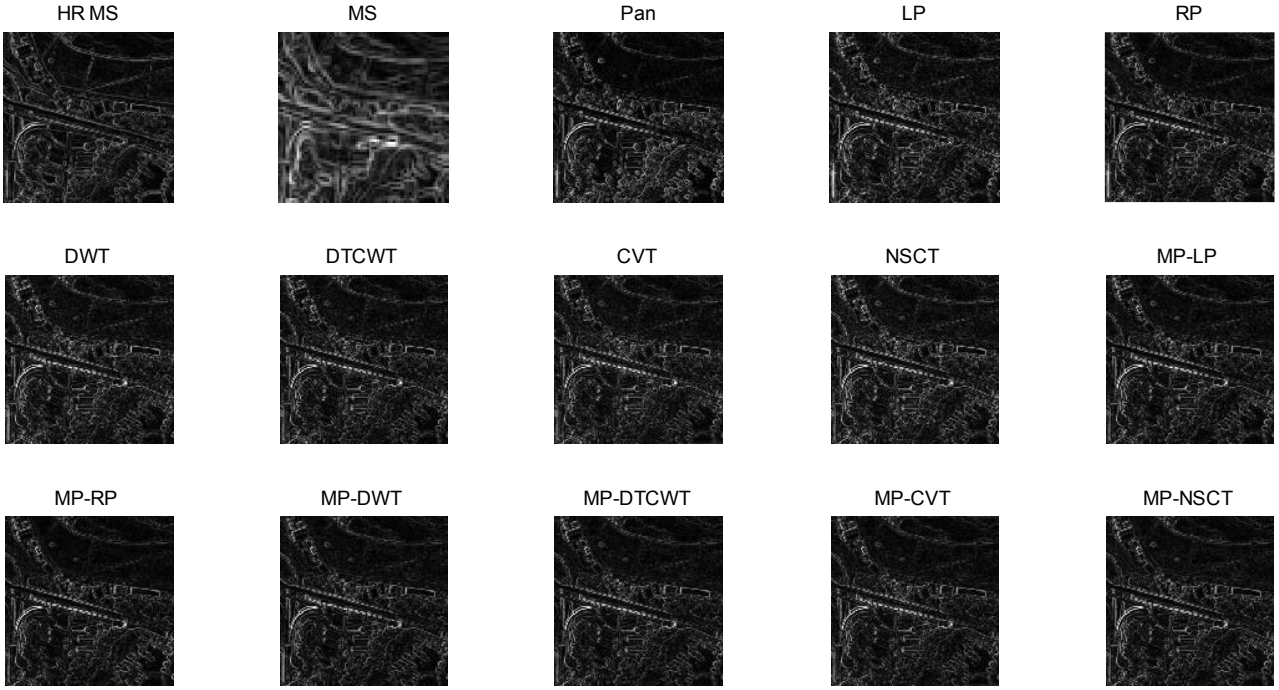

Fig. 18. Gradient energy maps of different fusion methods for IKONOS dataset.

The comparison between different pansharpening methods in terms of FMI metric is reported in Table 7. Generally, the MP-MST methods result in more FMI value with respect to MST methods. The MP-RP method provides the highest mutual information between the pansharpened image and the source images (MS and PAN).

The proposed schemes in [26], i.e., MF-TO-HPF, MF-TO-HPM, MF-LA and MF-HG are also compared to the proposed methods in this paper. The proposed schemes in [26] are compared with MP-RP in GeoEye dataset and with MP-DTCWT in QuickBird and IKONOS datasets. The results are reported in Tables 8-10. Among MF-TO-HPF,

Table 4. Gradient energies of different pansharpening methods for GeoEye dataset.

Method	Gradient energy	Method	Gradient energy	Method	Gradient energy
HR MS	6.5670 e+03	LP	6.6027 e+03	MP-LP	6.0294 e+03
MS	3.8803 e+03	RP	5.9674 e+03	MP-RP	5.5695 e+03
PAN	9.0458 e+03	DWT	6.7894 e+03	MP-DWT	6.2986 e+03
		DTCWT	6.2215 e+03	MP-DTCWT	5.6612 e+03
		CVT	6.4715 e+03	MP-CVT	5.7253 e+03
		NSCT	6.4994 e+03	MP-NSCT	5.9808 e+03

Table 5. Gradient energies of different pansharpening methods for QuickBird dataset.

Method	Gradient energy	Method	Gradient energy	Method	Gradient energy
HR MS	6.6560e+03	LP	11.0770e+03	MP-LP	9.6156e+03
MS	2.7040e+03	RP	9.6370e+03	MP-RP	8.7093e+03
PAN	11.2130e+03	DWT	10.3250e+03	MP-DWT	9.3577e+03
		DTCWT	10.0780e+03	MP-DTCWT	8.7859e+03
		CVT	9.9200e+03	MP-CVT	8.8938e+03
		NSCT	11.1340e+03	MP-NSCT	9.6085e+03

Table 6. Gradient energies of different pansharpening methods for IKONOS dataset.

Method	Gradient energy	Method	Gradient energy	Method	Gradient energy
HR MS	8.2548e+03	LP	8.8757e+03	MP-LP	8.0357e+03
MS	3.6508e+03	RP	7.9145e+03	MP-RP	7.4853e+03
PAN	8.4367e+03	DWT	8.7505e+03	MP-DWT	7.6461e+03
		DTCWT	8.3321e+03	MP-DTCWT	7.6265e+03
		CVT	8.4970e+03	MP-CVT	7.7365e+03
		NSCT	9.0765e+03	MP-NSCT	7.8913e+03

Table 7. FMI values of different pansharpening methods.

	LP	RP	DWT	DTCWT	CVT	NSCT	MP-LP	MP-RP	MP-DWT	MP-DTCWT	MP-CVT	MP-NSCT
GeoEye	0.8061	0.8230	0.8081	0.8073	0.8027	0.8033	0.8119	**0.8275**	0.8100	0.8117	0.8068	0.8111
QuickBird	0.7771	0.7937	0.7796	0.7797	0.7761	0.7732	0.7915	**0.8048**	0.7870	0.7889	0.7861	0.7928
IKONOS	0.8181	0.8241	0.8200	0.8185	0.8153	0.8198	0.8277	**0.8320**	0.8272	0.8279	0.8234	0.8303
WV2	0.8732	0.8754	0.8695	0.8722	0.8663	**0.8765**	0.8721	0.8725	0.8687	0.8708	0.8672	0.8742

Table 8. Comparison results of the proposed MP- MST methods with the proposed schemes in [26] for GeoEye dataset.

	Optimum values	MF-TO-HPF	MF-TO-HPM	MF-LA	MF-HG	Proposed (MP-RP)
RMSE	0	**0.0004**	**0.0004**	**0.0004**	**0.0004**	**0.0004**
ERGAS	0	0.0025	0.0026	0.0025	0.0025	**0.0021**
SAM	0	5.2576	5.2722	5.2134	5.001	**4.9289**
ρ	1	0.8912	0.8823	0.9011	**0.9053**	0.8810
D	0	0.0351	0.0362	0.0341	0.0338	**0.0326**
UIQI	1	0.8913	0.8857	0.8923	**0.8982**	0.8767

Table 9. Comparison results of the proposed MP- MST methods with the proposed schemes in [26] for QuickBird dataset.

	Optimum values	MF-TO-HPF	MF-TO-HPM	MF-LA	MF-HG	Proposed (MP-DTCWT)
RMSE	0	0.0009	0.0009	**0.0008**	**0.0008**	**0.0008**
ERGAS	0	0.0055	0.0060	0.0053	0.0053	**0.0049**
SAM	0	5.6018	5.6113	5.6012	5.5693	**5.5504**
ρ	1	0.8192	0.8189	0.8195	**0.8201**	0.8185
D	0	0.0904	0.0912	0.0901	**0.0875**	**0.0875**
UIQI	1	0.8168	0.8159	0.8169	0.8170	**0.8171**

Table 10. Comparison results of the proposed MP-MST methods with the proposed schemes in [26] for IKONOS dataset.

	Optimum values	MF-TO-HPF	MF-TO-HPM	MF-LA	MF-HG	Proposed (MP-DTCWT)
RMSE	0	**0.0004**	**0.0004**	**0.0004**	**0.0004**	**0.0004**
ERGAS	0	0.0023	0.0024	0.0023	0.0023	**0.0022**
SAM	0	5.2249	5.2331	5.2238	5.2105	**5.0894**
ρ	1	0.8923	0.8920	**0.9088**	**0.9088**	**0.9088**
D	0	0.0467	0.0468	0.0459	0.0452	**0.0441**
UIQI	1	0.8848	0.8823	0.8895	0.8960	**0.8963**

Table 11. Running time comparison.

	LP	RP	DWT	DTCWT	CVT	NSCT	MP-LP	MP-RP	MP-DWT	MP-DTCWT	MP-CVT	MP-NSCT
Running Time (seconds)	0.1340	0.1349	0.2525	0.2339	1.0829	3.1175	0.0545	0.2965	0.3085	0.4067	0.9726	3.1240

MF-TO-HPM, MF-LA and MF-HG methods, first MF-HG and then MF-LA provide the best results. As we can see, the proposed methods are generally provide better quality indices compared to MF-TO-HPF, MF-TO-HPM, MF-LA and MF-HG methods although the MF-HG method could provide the highest correlation coefficient in GeoEye and QuickBird data.

The running time of different pansharpening methods are reported in Table 11. As seen, the use of MP-version of methods increases the computation time in all methods except LP and CVT. The increased time in RP, DWT, DTCWT and NSCT is not significant. The reason can be explained as follows: applying closing operators on MS image and opening operators on PAN image can improve or even simplify the fusion process using MST.

5- CONCLUSION

A MP-MST method was proposed in this paper for pansharpening. The proposed method utilizes the useful characteristics of morphological by reconstruction operators to decrease the spatial redundancies, noise and distortion in the final fused product. Among different MP-MST methods (MP-LP, MP-RP, MP-DWT, MP-DTCWT, MP-CVT and MP-NSCT) generally MP-RP provides the best result in terms of quality indices with reference in GeoEye dataset while MP-DTCWT achieves the best values of quality indices in QuickBird and IKONOS datasets. In addition, the performance of MP-MST methods are assessed compared to a non-reference quality metric called FMI which measures the feature mutual information between source images and fused product. The results show that MP-RP provides the highest FMI value in all experimented datasets. It is worthful to note that the proposed MP-MST method can be implemented for fusion of other types of images in other fields although the performance of MP-MST is just assessed for remote sensing applications in this paper.

REFERENCES

[1] X. He, L. Condat, J. M. Bioucas-Dias, J. Chanussot, J. Xia,A New Pansharpening Method Based on Spatial and Spectral Sparsity Priors, *IEEE Transactions on Image Processing* 23 (9) (2014) 4160-4174.

[2] X. Zhou , J. Liu , S. Liu , L. Cao , Q. Zhou, H. Huang,A GIHS-based spectral preser- vation fusion method for remote sensing images using edge restored spectral modulation, ISPRS Journal of Photogrammetry and Remote Sensing 88 (2014) 16–27.

[3] J. Duran, A. Buades, B. Coll, C. Sbert, G. Blanchet, A survey of pansharpening methods with a new band-decoupled variational model, ISPRS Journal of Photogrammetry and Remote Sensing 125 (2017) 78-105.

[4] X. Luo, Z. Zhang, X. Wu, A novel algorithm of remote sensing image fusion based on shift-invariant Shearlet transform and regional selection, AEU - International Journal of Electronics and Communications 70 (2) (2016) 186-197.

[5] L. Alparone, S. Baronti, B. Aiazzi, A. Garzelli, Spatial Methods for Multispectral Pansharpening: Multiresolution Analysis Demystified, *IEEE Transactions on Geoscience and Remote Sensing* 54 (5) (2016) 2563-2576.

[6] W. Kong, Y. Lei, Y. Lei, X. Ni, Fusion technique for grey-scale visible light and infrared images based on non-subsampled contourlet transform and intensity-hue-saturation transform, *IET Signal Processing* 5 (1) (2011) 75-80.

[7] Shruti, S. Budhiraja, Multiscale image fusion for pansharpening of multispectral images using saliency detection, *2016 Ninth International Conference on Contemporary Computing (IC3)*, Noida (2016) 1-6.

[8] C. Theoharatos, V. Tsagaris, N. Fragoulis, G. Economou,Hyperspectral image fusion using 2-D principal component analysis, *2011 2nd International Conference on Space Technology*, Athens (2011) 1-4.

[9] Earth Resource Mapping Pty Ltd,The Brovey transform explained, EMU Forum, vol. 2, no. 11, 1990. Available at: http: // www. ermapper.com/ forum_new/emuf2-11.htm # aiticle_5 (last accessed 05.05.2013).

[10] A. Garzelli, F. Nencini, L. Capobianco,Optimal MMSE pan sharpening of very high resolution multispectral images, IEEE Transactions on Geoscience and Remote Sensing 46 (1) (2008) 228–236.

[11] C. L. Chien and W. H. Tsai,Image Fusion With No Gamut Problem by Improved Nonlinear IHS Transforms for Remote Sensing, in *IEEE Transactions on Geoscience and Remote Sensing*, 52 (1) (2014) 651-663.

[12] S. Zhong, Y. Zhang, Y. Chen, D. Wu,Combining Component Substitution and Multiresolution Analysis: A Novel Generalized BDSD Pansharpening Algorithm, IEEE Journal of Selected Topics in Applied Earth Observations and Remote Sensing 10 (6) (2017) 2867-2875.

[13] F. Palsson, J. R. Sveinsson, M. O. Ulfarsson, J. A. Benediktsson,Model-Based Fusion of Multi- and Hyperspectral Images Using PCA and Wavelets, *IEEE Transactions on Geoscience and Remote Sensing* 53 (5) (2015) 2652-2663.

[14] P.J. Burt, E.H. Adelson,The Laplacian pyramid as a compact image code, IEEE Transactions on Communications 31 (4) (1983) 532–540.

[15] A. Toet, Image fusion by a ratio of low pass pyramid, Pattern Recogn. Lett. 9 (4) (1989) 245–253.

[16] U. Yati, M. Biswas, Dual Discrete Wavelet Transform Based Image Fusion Using Averaging Principal Component, Recent Trends in Communication, Computing, and Electronics. Lecture Notes in Electrical Engineering 524 (2019).

[17] J. Lewis, R. OCallaghan, S. Nikolov, D. Bull, N. Canagarajah,Pixel and region based image fusion with complex wavelets, Inform. Fusion 8 (2) (2007) 119–130.

[18] F. Nencini, A. Garzelli, S. Baronti, L. Alparone, Remote sensing image fusion using the curvelet transform, Inform. Fusion 8 (2) (2007) 143–156.

[19] Q. Zhang, B. Guo,Multifocus image fusion using the nonsubsampled contourlet transform, Signal Process., 89 (7) (2009) 1334–1346.

[20] Yu Liu, Shuping Liu, Zengfu Wang, A general framework for image fusion based on multi-scale transform and sparse representation, Information Fusion 24 (2015) 147-164.

[21] M. Vega, J. Mateos, R. Molina, A. K. Katsaggelos, Super Resolution of Multispectral Images using ℓ1 Image Models and Interband Correlations, Journal of Signal Processing Systems for Signal, Image, and Video Technology 65 (3) (2011) 509–523.

[22] X. Yang, L. Jian, B. Yan, K. Liu, L. Zhang, Y. Liu, A sparse representation based pansharpening method, Future Generation Computer Systems, 88 (2018): 385-399.

[23] M. Imani, H. Ghassemian, Pansharpening Optimisation Using MultiResolution Analysis and Sparse Representation, International Journal of Image and Data Fusion 8 (3) 270–292, 2017.

[24] J. Qu, Y. Li, W. Dong, Fusion of hyperspectral and panchromatic images using an average filter and a guided filter, Journal of Visual Communication and Image Representation 52 (2018) 151-158.

[25] B. Aiazzi, L. Alparone, S. Baronti, A. Garzelli, M. Selva, MTF-tailored multiscale fusion of high-resolution MS and Pan imagery, Photogramm. Eng. Remote Sens. 72 (5) (2006) 591–596.

[26] R. Restaino, G. Vivone, M. Dalla Mura, and J. Chanussot, Fusion of Multispectral and Panchromatic Images Based on Morphological Operators, IEEE Transactions on Image Processing, 25 (6) (2016): 2882- 2895.

[27] F. Laporterie, O. Amram, G. Flouzat, E. Pilicht, and M. Gayt, Data fusion thanks to an improved morphological pyramid approach: comparison loop on simulated images and application to SPOT 4 data, *Proc. IEEE IGARSS*, (2000) 2117–2119.

[28] M. Imani, H. Ghassemian, Edge patch image-based morphological profiles for classification of multispectral and hyperspectral data, *IET Image Processing* 11 (3) (2017) 164-172.

[29] A.-G. Legaz-Aparicio, R. Verdu-Monedero, J. Angulo, Adaptive morphological filters based on a multiple orientation vector field dependent on image local features, Journal of Computational and Applied Mathematics 330 (2018) 965-981.

[30] P. J. Burt, R. J. Kolezynski, Enhanced image capture through fusion, in Proc. International Conference on Computer Vision (1993) 173-182.

[31] A. Toet, Image fusion by a ratio of low-pass pyramid, Pattern Recognition Letters 9 (4) (1989) 245-253.

[32] R. C. Gonzalez, R. E. Woods, Digital Image Processing (3rd Edition), Prentice-Hall, Inc. Upper Saddle River, NJ, USA, 2006.

[33] R. Raj Singh, R. Mishra, Benefits of Dual Tree Complex Wavelet Transform over Discrete Wavelet Transform for Image Fusion, International Journal for Innovative Research in Science & Technology 1 (11) (2015) 259-263.

[34] T. S. Anand, K. Narasimhan, P. Saravanan,Performance evaluation of image fusion using the Multi-Wavelet and Curvelet transforms, *IEEE-International Conference On Advances In Engineering, Science And Management (ICAESM -2012)*, Nagapattinam, Tamil Nadu (2012) 121-129.

[35] M. Dalla Mura, J. A. Benediktsson, B. Waske, L. Bruzzone, Extended profiles with morphological attribute filters for the analysis of hyperspectral data, Int. J. Remote Sens., 31 (22) (2010) 5975–5991.

[36] G. Vivone *et al*.,A Critical Comparison Among Pansharpening Algorithms, *IEEE Transactions on Geoscience and Remote Sensing* 53 (5) (2015) 2565-2586.

[37] M. B. Akbari Haghighat, A. Aghagolzadeh, H. Seyedarabi, A non-reference image fusion metric based on mutual information of image features, Computers & Electrical Engineering 37 (5) (2011) 744-756.

[38] M. Imani, H. Ghassemian, Binary coding based feature extraction in remote sensing high dimensional data, Information Sciences 342 (2016) 191-208.

HOW TO CITE THIS ARTICLE

M, Imani, A Multi-Scale Transform Method Based on Morphological Operators for Pansharpening, AUT J. Model. Simul., 52(1) (2020) 97-116.

DOI: 10.22060/miscj.2020.17306.5178